Electron cooling: Status and perspectives

I. N. Meshkov
Joint Institute for Nuclear Research, Dubna

Fiz. Elem. Chastits At. Yadra **25**, 1487–1560 (November–December 1994)

Electron cooling, which has now become a conventional tool in accelerator technology, makes it possible to form intense, dense beams with low emittance and small particle momentum spread in storage rings for heavy charged particles. Nine such storage rings, referred to as coolers, are presently operating in laboratories in Europe, the United States, and Japan; one of these is an antiproton storage ring, and the other eight are ion rings. These have greatly expanded the experimental possibilities in the study of elementary-particle and nuclear physics. This review is devoted to the current status of the electron cooling method and its applications. Special attention is given to the description and analysis of the results of experiments on the cooling of multiply charged ions which have been performed recently. The physics of the method is described in order to systematize the existing physical ideas, and to facilitate acquaintance with the subject for those unfamiliar with it.

I. INTRODUCTION

The method of electron cooling has been under development for almost thirty years, beginning from the first idea of Budker,[1] based on the model of a two-component electron–ion plasma, and leading to the now very rich physics of collisions in a magnetized electron beam with a "flattened" electron velocity distribution. The method allows an effective friction to be created in a beam of charged particles which decreases the three-dimensional phase space: the emittance of the beam and the energy spread of the beam particles. As a result, a dense and cold beam of heavy charged particles is formed.

The idea of Budker arose in the course of seeking a way of increasing the density and, accordingly, the luminosity of colliding proton–proton beams. Later (owing to a suggestion of Skrinskiĭ) it was realized that the storage of antiprotons and the realization of colliding pp beams were possible.[2]

In contrast to "radiation cooling," where the phase space of the beam is reduced owing to losses of the particle energy to radiation, in electron cooling an extraneous energy "absorber" is introduced into the beam.

It is possible in principle to use as this absorber atomic electrons and, accordingly, ionization losses as the friction mechanism. Unfortunately, nature has not been so generous: ionization friction[3] does not work for baryons, because particle losses in strong interactions with the nuclei of the absorber material sharply limit the lifetime of the beam.[1)] Nevertheless, ionization friction is today viewed as a method of practical interest for cooling heavy lepton beams (muon cooling; see the articles in Ref. 4).

The idea of Budker had two remarkable features: first, free elecrons (an "electron gas") are used as the absorber, and, second, the average velocity of these electrons coincides with the average velocity of the cooled particles.[2)] This ultimately led to the idea of "intersecting" (not colliding head-on, but while passing each other) beams—a cooled particle beam and a cooling electron beam. It was necessary to be rather bold (if not impudent!) to attempt to realize this idea.

Electron cooling was first realized in 1974 in experiments on cooling a beam of protons of energy 68 MeV at the NAP-M storage ring at the Nuclear Physics Institute (NPI) in Novosibirsk.[5]

Fortunately, electron cooling was successful from the very beginning: the scheme with transport of the electron beam in a longitudinal magnetic field chosen for the first cooling system[6,7] proved to be very effective. Moreover, it made it possible to form an intense electron beam with small angular spread and extremely low electron losses, because it turned out that in cooling by "magnetized" electrons the rate and depth of cooling are increased sharply. This effect was discovered experimentally,[8] and research into it, begun in the late 1970s,[3,9,10] continues to this day and gives more and more new information about the nature of charged-particle beams.

The history of the discovery of this effect is curious and quite instructive. The first experiments[5] gave good agreement with the predictions of the pioneering work of Budker.[1] In the next series of studies, carried out after the stability of the electron energy and the uniformity of the magnetic field had been improved, a cooling time lower by an order of magnitude was obtained.[8] This discovery provided the impetus to the development of ideas about the structure of the electron beam (the "flattened" distribution, electron relaxation effects, and so on; see Sec. 4 below) and its effect on the efficiency of electron cooling (Secs. 1.3 and 1.4).

In the late 1970s and early 1980s electron cooling of protons was successfully demonstrated at CERN[11] and at Fermilab.[12] The method was developed further up to the mid-1980s. Then the first experiments were performed to study deeply cooled beams, and the effects of the ordering of the particle locations along the longitudinal degree of freedom were discovered.[13] These studies initiated a new direction in beam physics: "crystalline beams" (Ref. 14), which continues to be an active area today.

Nevertheless, until the mid-1980s, in spite of the many promising suggestions (see Refs. 9 and 15, for example), electron cooling did not find any real practical applications. Its opponents were even inclined to consider the method as no more than a pretty "game" with no practical use. This

was underlined in particular by the great advances attained at CERN using the method of stochastic cooling proposed by van der Meer also at the beginning of the 1960s.[16] Antiproton storage using this method made it possible to create the proton–antiproton collider at which the carriers of the weak interaction, the W and Z bosons, were first discovered. The situation changed in the late 1980s and early 1990s, when, one by one, ion storage rings with electron cooling, referred to as coolers, came into operation (Table I). Some idea of the possibilities that they offer can be gleaned from the results of experiments on the storage and cooling of ion beams (Table II; Ref. 17). The fundamental design of the cooler has not undergone any significant changes since the first such storage ring NAP-M (the Russian acronym for Antiproton Storage Ring Model; Fig. 1) and its electron-cooling system EPOKhA (the Russian acronym for Electron Beam, Cooling Antiprotons; Fig. 2) were built at NPI (Refs. 6 and 7): the storage ring has two (or more) straight segments, one of which is used to extract the electron beam with the beam of cooled particles. The electrons are transported in a longitudinal magnetic field from the cathode of the gun via the cooling segment to the collector, which is at a potential slightly higher than that of the cathode (the energy recuperation scheme). The cooled particles circulating in the storage ring pass through the cooling segment repeatedly, interacting each time with a fresh set of electrons. In this regard the cooling system is analogous to a refrigerator in which the electron beam plays the role of the coolant transferring heat from the heated body—the particle beam—to the acceptor—the source of the voltage between the cathode of the electron gun and the electron collector.

The electron cooling technique is developing in several directions, which have the common goal of increasing the efficiency and broadening the range of applications. Examples are (see Ref. 4):

- the generation of electron beams with the maximum current density at the minimum attainable electron temperature: electron guns with "adiabatic optics," "adiabatic acceleration," photocathodes;
- the generation of electron beams in devices with neutralization of the electron space charge;
- the same in an adiabatically slowly decreasing magnetic field, which makes it possible to decrease the transverse temperature of the electrons (by increasing the longitudinal temperature);
- broadening of the electron energy range into the MeV region;
- the creation of efficient electron energy recuperators.

The appearance of coolers in nuclear research has revealed qualitatively new possibilities: the performance of precision experiments in beams with extremely small (down to 10^{-6}) energy spread and superthin internal targets (Sec. 7.2), mass spectrometry of superhigh resolution (Sec. 7.3), and the separation and storage of long-lived isotopes and isomers (Sec. 7.3).

Similar possibilities have arisen also in atomic physics, where, in particular, the cooling electron beam is used as the "target." Here we should mention "laser cooling," which has become a reality owing to cold ion beams in coolers (Sec. 7.4).

Electron cooling has led to the development of a second new direction in the physics of charged-particle beams, that of the so-called crystalline beams (Refs. 13 and 14), which are of great interest for solid-state physics as a model of a crystal (Sec. 6.2).

Electron cooling today has not only not lost its value as a method for the storage and production of charged-particle beams, but has become foremost in importance. In the competition with stochastic cooling the regions of applicability of each of these methods are clearly defined. Stochastic cooling is most useful for the primary cooling of beams with large emittance (100π mm mrad and more) and moderate

TABLE I. Storage rings with electron cooling.

Storage ring	NAP-M, Novosibirsk	ICE CERN	Test Ring FLAB	LEAR CERN	MOSOL, Novosibirsk	IUCF COOLER Bloomington	TSR Heidelberg	TARN-II Tokyo
Perimeter, m	47	74	1.35	78.6	length 3m	86.8	55.4	77.8
Magnetic field strength, T·m	1.5	1.0	2.1	2		3.6	1.5	6.1
Particle energy, MeV/nucleon	1.5–85	46	200	64	0.85	500	30	100
Type of ion	p	p	p	p	p, H^-	$A\leqslant 7$	$A\leqslant 127$	$A\leqslant 20$
Horizontal acceptance, π mm mrad	80	60		100		25	500	260
Vertical acceptance, π mm mrad	80	30		48		25	120	15
Longitudinal acceptance, $\Delta p/p$, %	1.0	0.5		0.5		±0.2	±3	±0.1
Length of cooling section, m	1	1.5			2.4	2.8	1.5	1.5
Q_h	1.2			2.305		4.15	2.75	1.75
Q_v	1.4			2.73		5.15	2.825	1.8
β_h in cooling section, m	5.5			1.9		2.3	5.5	10
β_v in cooling section, m	5.5			5.3		4	5.7	4
Dispersion in cooling section, m				3.6		0	0–1	4.7
γ_{tr}	1.117			$\sqrt{-22}$		4.85	2.96	1.88
Operation with electron cooling	1974–84	1979–80	1980–82	c 1988	1986–88	c 1988	c 1988	c 1989
Beam diameter, cm	1	5	5	5	0.2	2.54	5	5
Electron beam energy, keV	0.8–46	26	111	35	0.470	10–270	3–20	$\leqslant 130$
Electron beam current, A	0.02–08	2.2	3.0	3.0	0.015	0–4.8	1	$\leqslant 10$
Magnetic field, kG	1.0	0.6		0.6		1–1.5	0.55	1.2
Vacuum in cooling section, Torr	5×10^{-10}	2×10^{-9}	1×10^{-10}	2×10^{-12}	1×10^{-10}	1×10^{-9}	$<10^{-11}$	10^{-11}

TABLE I. (Continued)

Storage ring	ASTRID Aargus	ESR Darmstadt	CELSIUS Uppsala	CRYRING Stockholm	COSY Julich	K4, Dubna	K10 Dubna
Perimeter, m	40	108.4	81.8	51.6	184	83.12	146.24
Magnetic field strength, T·m	1.87	10	7	1.44	11	4	10
Particle energy, MeV/nucleon	50	30–560	340(1360)	0.3–24	40–2500	170	330
Type of ion		$A \leqslant 238$	$A \leqslant 40$		p	$A \leqslant 238$	$A \leqslant 238$
Horizontal acceptance, π mm mrad		450	120	200	180	50	25
Vertical acceptance, π mm mrad		150	120	100	36	50	25
Longitudinal acceptance, $\Delta p/p$, %		±2	±0.3	±1.7	±0.5	1.0	2.0
Length of cooling section, m		2.5	2.5	1.1	2	2.5	2.5
Q_h	2.29	2.1–2.45	1.68	2.3	3.38	2.4	2.8
Q_v	2.73	2.1–2.45	1.9	2.27	3.38	2.8	3.3
β_h in cooling section, m		8	8.14	2.3	10	10.9	5.6
β_v in cooling section, m		8–10	5.04	2.9	10	6.3	5.8
Dispersion in cooling section, m		0–6	1.48	1.6	0	0	0
γ_{tr}		2.7	2.605	2.23	2.2	5.26	2.36
Operation with electron cooling	1993	1990	1989	1992	1992	1996	1997
Beam diameter, cm		5	2	4	2.54	3	3
Electron beam energy, keV	27	10–320	10–300	2–20	100	15–100	100–250
Electron beam current, A	3	0.5–5	0–2.8	0.001–3	3	0.8–5	6
Magnetic field, kG		0.1–2.5	0.5–2	2.5	0.8	1–2	2
Vacuum in cooling section, Torr	10^{-12}	$<10^{-10}$	10^{-11}	10^{-11}	1×10^{-10}	1×10^{-9}	1×10^{-9}

intensity, especially if deep cooling to low values of the emittance and small energy spread is not required, and it is insensitive to the particle energy. Electron cooling is most useful for creating and storing intense beams with relatively small emittance; it is the only method of obtaining deeply cooled beams with large space-charge density.

The electron cooling method can also be used to cool positron beams,[18] which makes it possible to construct an effective generator of antihydrogen atoms (Sec. 8).

Our discussion in this review is limited to heavy-particle energies of the order of 500 MeV/nucleon. A separate problem which we do not consider here is that of electron cooling at ultrarelativistic energies, where at present the only possible "refrigerator" is a special electron storage ring in which low electron temperature is ensured by radiation friction.[19,20] This problem has so far only been studied theoretically.

In order to give an idea of the typical numbers, in this review we present numerical estimates for a "typical" storage ring with electron cooling, the parameters of which are given in Table III.

TABLE II. Parameters of ion beams stored in coolers.

Storage ring	Ion	Energy, MeV/nucleon	N	I mA
LEAR	O^{5+}	12.5	1×10^{9}	0.8
TSR	C^{6+}	6.1	3.7×10^{10}	18
	Si^{14+}	4.1	6×10^{8}	1.0
	S^{16+}	6.1	8×10^{8}	1.5
ESR	Ne^{10+}	250	2.5×10^{8}	7.0
	Ar^{18+}	250	4×10^{8}	2.0
	Kr^{36+}	150	1×10^{8}	0.9
	Xe^{54+}	250	4×10^{8}	6.0
	Dy^{66+}	297	1×10^{8}	2.0
	Au^{79+}	300	4×10^{8}	0.1
	Bi^{82+}	230	5×10^{8}	1.2
TARN-II	N^{7+}	---	1×10^{6}	---
CELSIUS	O^{8+}	---	3×10^{8}	---

1. THE PHYSICS OF ELECTRON COOLING

1.1. A heavy particle in an electron gas

The electron cooling scheme presupposes that the average velocities of the particles of the cooled beam and of the cooling electrons are equal or slightly different. Therefore, for describing the interaction it is convenient to go to the "electron frame" moving with the average electron velocity $\vec{v}_0$. A particle which has velocity $\vec{V}$ in this frame undergoes Coulomb collisions with the electrons (whose velocity is $\vec{v}$), and the effect of these collisions is completely analogous

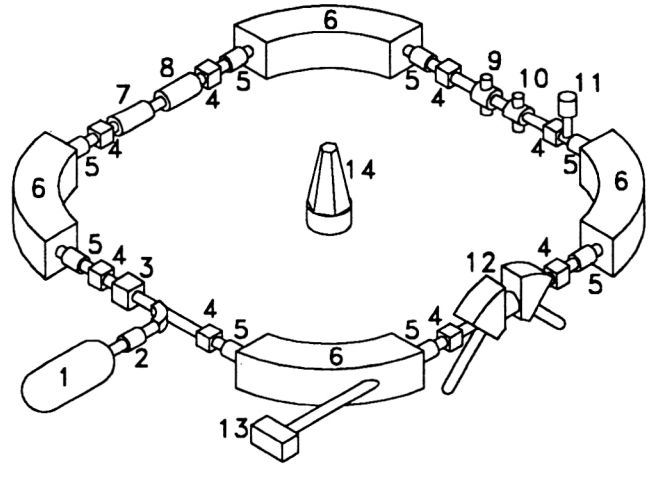

FIG. 1. Schematic diagram of the NAP-M storage ring: *1*—injector; *2*—injection channel; *3*—inflector; *4*—pickup station; *5*—quadrupole lens; *6*—bending magnet; *7*—accelerating resonator; *8*—excitation deflector of betatron oscillations; *9*—quartz filament intersecting the beam; *10*—magnesium vapor jet; *11*—scintillation counter for recording protons scattered by the filament; *12*—electron cooling setup; *13*—detector of neutral hydrogen atoms (two-coordinate proportional chamber); *14*—geodesic signal.

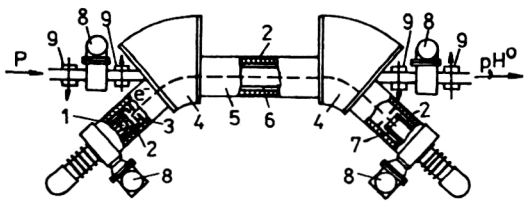

FIG. 2. Schematic diagram of the EPOKhA setup: *1*—electron gun; *2*—straight solenoids; *3*—anodes of electron gun; *4*—toroidal solenoids; *5*—cooling section; *6*—vacuum chamber; *7*—electron beam collector; *8*—vacuum pumps; *9*—dipoles correcting the proton trajectory (pp'); H^0—yield of hydrogen atoms.

to the ionization losses in the motion of a charged particle in a medium. Therefore, the expression for the friction force acting on a particle with charge ze in an ultracold electron gas can be written down directly:

$$\vec{F}=\frac{\vec{V}}{V}\frac{d\mathscr{E}}{dx}=-\frac{\vec{V}}{V}\frac{4\pi qL_C}{mV^2}, \tag{1.1}$$

$$q=n_e z^2 e^4, \quad L_C=\ln(\rho_{\max}/\rho_{\min}), \tag{1.2}$$

where n_e is the electron density, m and e are the electron mass and charge, L_C is the Coulomb logarithm, and $\rho_{\max}$ and $\rho_{\min}$ are the maximum and minimum values of the impact parameter of the Coulomb collisions. It is usually assumed that

$$\rho_{\min}=\frac{ze^2}{mV^2}\approx(1-3)\cdot 10^7 z \text{ cm}, \tag{1.3}$$

TABLE III. Typical parameters of a storage ring with electron cooling.

Energy of cooled particles MeV/nucleon	55
Parameters of electron beam	
Electron energy, keV	30
Average velocity, cm/sec	1×10^{10}
Beam diameter, cm	3
Current density, A/cm^2	0.5
Plasma frequency, sec^{-1}	1×10^9
Average distance between electrons, cm	1.5×10^{-3}
Angular spread, mrad	3
Spread in electron transverse velocity, cm/sec	3×10^7
Electron transverse temperature, eV	0.5
Spread in electron longitudinal velocity, cm/sec	4×10^5
Longitudinal electron temperature, eV	2×10^{-4}
Magnetic field of cooling system, kG	1.0
Electron cyclotron frequency, sec^{-1}	1.8×10^{10}
Electron plasma frequency, sec^{-1}	1×10^9
Parameters of particle beam before cooling	
Angular spread, mrad	5
Momentum spread,	5×10^{-3}
Particle velocity in electron frame, cm/sec	5×10^7
Storage-ring parameters	
Perimeter C, m	75
Particle revolution period, μsec	0.75
Length of cooling segment l_{cool}, m	1.5
$\eta=l_{\text{cool}}/C$	0.02
Acceptance, mm·mrad	40π
Betatron and dispersion functions, m	5.0
Vacuum, Torr	1×10^{-10}

which corresponds to the scattering of an electron colliding with a particle at an angle of order $\pi/2$.

In a medium where a particle collides with atomic electrons it is natural to take $\rho_{\max}$ to be of the order of the atomic size, i.e., $\rho_{\max}\approx e^2/\varepsilon_{\text{ion}}$. This leads to the well known expression for the ionization losses of a nonrelativistic particle.

In an electron gas $\rho_{\max}$ is restricted by the minimum of three parameters:

$$\rho_{\max}=\min\begin{cases} a & \simeq 1.5 \text{ cm} \\ R_D\equiv\dfrac{\langle|\vec{U}|\rangle}{\omega_{pe}} & \simeq 0.05 \text{ cm} \\ \langle|\vec{U}|\rangle\cdot\tau & \simeq 0.5 \text{ cm}, \end{cases} \tag{1.4}$$

where a is the radius of the electron beam (the "cloud"), R_D is the Debye screening length,

$$\omega_{pe}=\sqrt{4\pi n_e e^2/m}\approx 10^9 c^{-1} \tag{1.5}$$

is the electron plasma frequency,

$$\vec{U}=\vec{V}-\vec{v} \tag{1.6}$$

is the relative velocity of the particle and the electron colliding with it in the electron frame, and τ is the time of passage of the particle through the cooling segment. The first criterion is obvious, the second gives an estimate of the distance over which the electrons "feel" the particle charge in the electron gas, and the third follows from the classical collision scheme, which gives the duration $\Delta t\approx\rho/|\vec{U}|$. The estimates (1.3) and (1.4) give $L_C\approx 15$. Equation (1.1) is valid for a sufficiently cold electron gas, in which

$$\sqrt{\langle v^2\rangle}\equiv\Delta_e\ll V.$$

In general it is necessary to take into account the electron velocity distribution, which obviously leads to the expression for the friction force:

$$\vec{F}=-\frac{4\pi qL_C}{m}\int_v\frac{\vec{U}}{U^3}f(\vec{v})d^3v, \quad \vec{U}=\vec{V}-\vec{v}. \tag{1.7}$$

The integral runs over the space of electron velocities. Here the weak logarithmic dependence of L_C on $\vec{v}$ is neglected.

An important feature of Eq. (1.7) is its complete analogy with the expression for the Coulomb field of a set of charges with density

$$\rho_{\text{equ}}=-\frac{4\pi qL_C}{m}f(\vec{v}). \tag{1.8}$$

This analogy makes it possible to simplify considerably the calculation of the friction force in specific cases (see below). In particular, we can immediately identify the two special cases of large and small particle velocities:

$$\vec{F}=(\vec{v}_p)\simeq-\frac{4\pi qL_C}{m}\times\begin{cases}\dfrac{\vec{V}}{V^3}, & V\gg\Delta_e \\ \dfrac{\vec{V}}{\Delta_e^3}, & V\ll\Delta_e. \end{cases} \tag{1.9}$$

The friction force is obviously maximal near $V\approx\Delta_e$ (see Fig. 7 below).

In collisions with electrons the momentum transferred to a particle can be split into two components, one along and one perpendicular to $\vec{U}$, the vector corresponding to the relative velocity of the particles before collision. The value of the longitudinal component averaged over many collisions gives the friction force (1.7), while the average value of the perpendicular component is zero. However, the mean square of the latter is nonzero, and physically this is none other than multiple scattering on electrons, or the process of transverse diffusion. This is seen particularly clearly for the example of a cold electron gas, when the particle velocity vector $\vec{v}_p$ deviates with time from the initial direction as $\sqrt{t}$. Using the well known expression for multiple scattering, we can write down the following, taking into account the electron velocity spread:

$$\frac{d\langle p_x^2\rangle}{dt}=\frac{d\langle p_y^2\rangle}{dt}=4\pi qL_C\int_v\frac{f(v)}{U}\,d^3v, \tag{1.10}$$

where x and y are the directions of the coordinate axes orthogonal to the initial direction of the particle velocity $\vec{V}=\vec{e}_Z V$. These expressions can naturally be obtained as a result of rigorous analysis of the process of particle collisions with electrons (see Ref. 21 for more details). In the general case of arbitrary orientation of the coordinate axes relative to the initial direction of the vector $\vec{V}$, instead of (1.10) we obtain the diffusion tensor (Refs. 10, 20, and 21):

$$D_{\alpha\beta}=\frac{d\langle\Delta p_\alpha\Delta p_\beta\rangle}{dt}=4\pi qL_C\int_v\frac{U^2\delta_{\alpha\beta}-U_\alpha U_\beta}{U^3}$$
$$\times f(\vec{v})d^3v. \tag{1.11}$$

For the case of an isotropic electron velocity distribution this tensor has only three nonzero components along its principal diagonal. Their sum gives the rate of change of the total energy of the particle (with mass M):

$$\frac{d\langle\mathscr{E}\rangle}{dt}=\frac{1}{2M}\frac{d(p^2)}{dt}=\frac{1}{2M}\sum_{\alpha=1}^{3}D_{\alpha\alpha}$$
$$=\frac{4\pi qL_C}{M}\int\frac{f(v)}{U}\,d^3v. \tag{1.12}$$

However, this is heating and not cooling generated by the friction force (1.7). What is going on? The answer follows from the overall picture of the behavior of a particle in an electron gas: under the action of the friction force (1.7) the particle loses its velocity, which on the average falls to zero, i.e., the particle is stopped. Further collisions with "hot" electrons produce fluctuations in the particle velocity, the mean square of which is also limited by friction-cooling. Therefore, the behavior of this velocity (momentum) component of the particle is described by a balance equation (the Langevin equation):

$$\frac{1}{2M}\frac{d\overline{\Delta p_\alpha^2}}{dt}=\overline{P}_\alpha+\overline{Q}_\alpha,\quad \alpha=1,2,3,$$

$$P_\alpha=F_\alpha v_\alpha,\quad Q_\alpha=\frac{1}{2M}\sum_\beta D_{\alpha\beta}. \tag{1.13}$$

Here the overline denotes time averaging, P_α is the power, α are the components of the friction force, and Q_α is the power of diffusion heating for the component.

It is obvious how to go from one particle to a beam passing through the electron gas: one goes from an average over time to an average over particles:

$$\frac{1}{2M}\frac{d}{dt}\langle\Delta p_\alpha^2\rangle=\langle P_\alpha\rangle+\langle Q_\alpha\rangle. \tag{1.14}$$

1.2. An isotropic gas of "Maxwellian" electrons

The equations of the preceding section can be integrated analytically also in the case of an isotropic Maxwellian velocity distribution of the particles and electrons:

$$f(\vec{v})d^3v=\left(\frac{M}{2\pi T}\right)^{3/2}e^{-\mu v^2/2T}v^2dvd\Omega\,,$$

$$T=\begin{cases}T_p\\T_e,\end{cases}\qquad \vec{v}=\begin{cases}\vec{V}\\\vec{v}\,,\end{cases}\qquad \mu=\begin{cases}M-\text{particles}\\m-\text{electrons}\,,\end{cases}$$

$$T\equiv\mu\Delta^2,\quad \Delta^2=\langle v_\alpha^2\rangle,\quad \alpha=\{x,y,z\}. \tag{1.15}$$

Since the distribution function is isotropic, it is convenient to use the Coulomb analogy. In this case the friction force (1.7) is analogous to the electric field of a system of charges with isotropic density distribution (1.8) and (1.15). Use of the Gauss theorem gives

$$\vec{F}_{\text{Maxw}}(\vec{V})=-\frac{\vec{V}}{V^3}\frac{4\pi qL_C}{m}\varphi(V), \tag{1.16}$$

where the universal function $\varphi(x)$ is expressed in terms of the error function:

$$\varphi(x)=\sqrt{\frac{2}{\pi}}\int_0^x e^{-y^2/2}dy-\sqrt{\frac{2}{\pi}}\,xe^{-x^2/2},$$

$$x=\sqrt{\frac{mV^2}{T_e}}=\frac{V}{\Delta_e}. \tag{1.17}$$

The function $\varphi(x)$ has a maximum at the point $x=1.3675$, and its asymptotes give, like (1.9),

$$\vec{F}_{\text{Maxw}}(\vec{V})\approx-\frac{4\pi qL_C}{m}\times\begin{cases}\dfrac{\vec{V}}{V^3}, & V_p\gg\Delta_e,\\[2ex] \sqrt{\dfrac{2}{9\pi}}\cdot\dfrac{\vec{V}}{\Delta_e}, & v_p\ll\Delta_e.\end{cases} \tag{1.18}$$

The power of the friction force averaged over the ensemble of Maxwellian particles is obtained by averaging over particles:

$$P_{\text{Maxw}}=\left\langle\sum_{\alpha=1}^{3}F_\alpha V_\alpha\right\rangle=\int_V(\vec{F}_{\text{Maxw}}\cdot\vec{V})\cdot f(\vec{V})d^3V.$$

Substituting (1.16) and (1.17) into this and integrating by parts, we find

$$P_{\text{Maxw}}=-\frac{4\sqrt{2\pi}qL_C}{Mm}\frac{T_p}{((T_p/M)+(T_e/m))^{3/2}}. \tag{1.19}$$

The power of diffusion heating is calculated analogously:

$$Q_{\text{Maxw}}=\frac{1}{2M}\left\langle \sum_{\alpha,\beta=1}^{3} D_{\alpha\beta}\right\rangle$$
$$=\frac{4\pi qL_C}{M}\int_V f(\vec{V})\int \frac{f(\vec{V})}{U}\,d^3v\,d^3V.$$

The variable substitution $\vec{x}=\vec{V}-\vec{v}$, $\vec{y}=\vec{V}+\vec{v}$ simplifies the integration procedure, which gives

$$Q_{\text{Maxw}}=\frac{4\sqrt{2\pi}qL_C}{M}\left(\frac{T_p}{M}+\frac{T_e}{m}\right)^{-1/2}. \tag{1.20}$$

Substitution of the resulting expressions (1.19) and (1.20) into the Langevin equation (1.14) leads to the relaxation equation for a two-component plasma:[22]

$$\frac{dT_p}{dt}=\frac{8\sqrt{2\pi}qL_C}{3Mm}\frac{T_p(1-m/M)-T_e}{((T_p/M)+(T_e/m))^{3/2}}=-\frac{dT_e}{dt}. \tag{1.21}$$

Neglecting the term m/M, from this we obtain the equilibrium condition:

$$T_p=T_e,\quad \Delta_p=\sqrt{\frac{m}{M}}\cdot\Delta_e\ll\Delta_e. \tag{1.22}$$

Therefore, the two-component particle-plus-electron plasma relaxes to the equilibrium state of equal temperatures (which is almost obvious from general thermodynamical considerations). The last inequality in (1.22) emphasizes the meaning of the idea of electron cooling: the spread in particle velocities is much smaller than the spread in electron velocities.

It follows from (1.21) that the maximum cooling velocity is reached for

$$T_p\approx\frac{2M}{m}T_e \quad\text{or}\quad \Delta_p=\sqrt{2}\Delta_e,$$

$$\left(\frac{dT_p}{dt}\right)_{\max}=-\frac{16\sqrt{2\pi}}{9\sqrt{3}}\frac{qL_C}{\sqrt{mT_e}}.$$

Equation (1.21) has a simple solution for the two limiting cases of large and small ν_p. For fixed electron temperature (which is typical of the electron cooling scheme), from (1.21) we find

$$T_p(t)=\begin{cases} T_p\left(1-\dfrac{t}{\tau_{\text{Maxw}}}\right)^{2/3}, & \Delta_p\gg\Delta_e \\ T_e+(T_p-T_e)e^{-t/\tau_{\text{Maxw}}}, & \Delta_p\ll\Delta_e, \end{cases}$$

where τ_{Maxw} is the cooling time, in this case for Maxwellian particles in an isotropic gas of Maxwellian electrons:

$$\tau_{\text{Maxw}}=\frac{mM}{4\sqrt{2\pi}q}\times\begin{cases}(\Delta_p^0)^3, & \Delta_p\gg\Delta_e, \\ \frac{3}{2}\Delta_e^3, & \Delta_p\ll\Delta_e. \end{cases} \tag{1.23}$$

Here the superscript 0 labels the initial values of the parameters.

It should be noted that various definitions are used in the literature for the concept of "cooling time." Sometimes this refers to the instantaneous value of the inverse decrement:

$$\tau_{\text{inst}}=\left(-\frac{1}{T_p}\frac{dT_p}{dt}\right)^{-1}. \tag{1.24}$$

To avoid confusion, in what follows for the instantaneous value of (1.24) we shall use the term "inverse decrement." Equation (1.24) for a Maxwellian plasma gives the expression for the relaxation time of a two-component plasma commonly found in the literature:[21]

$$(\tau_{\text{Maxw}})_{\text{inst}}=\frac{3Mm}{8\sqrt{2\pi}qL_C}\left(\frac{T_p}{M}+\frac{T_e}{m}\right)^{3/2}=\frac{3}{8\sqrt{2\pi}q}$$
$$\times\begin{cases}\Delta_p^3, & \Delta_p\gg\Delta_e \\ \Delta_e^3, & \Delta_p\ll\Delta_e. \end{cases} \tag{1.25}$$

This is the equation that Budker used in his first study on electron cooling.[1]

1.3. A particle in the electron beam. The "flattened" distribution

The cooling of a particle beam in a gas of Maxwellian electrons is a simple physical model convenient for an elementary explanation of the nature of the phenomenon. However, if the electron beam is obtained by acceleration in an electrostatic field, the velocity distribution of its electrons is significantly anisotropic in the electron frame: the spread in longitudinal velocities is much smaller than the spread in transverse ones. A sufficiently good approximation of this anisotropic distribution function is the Maxwellian function[23]

$$f(\vec{v})d^3v=\left(\frac{m}{2\pi}\right)^{3/2}\frac{1}{T_\perp\sqrt{T_\parallel}}\,e^{-mv_\perp^2/2T-mv_\parallel^2/2T}$$
$$\times 2\pi v_\perp dv_\perp dv_\parallel,$$
$$\tfrac{1}{2}m\langle v_\perp^2\rangle=\tfrac{1}{2}m(\langle v_x^2\rangle+\langle v_y^2\rangle)\equiv m\Delta_\perp^2=T_\perp\approx T_c\geqslant 0.1\ \text{eV},$$
$$m\langle v_\parallel^2\rangle\equiv m\Delta_\parallel^2=T_\parallel\approx\frac{T_c^2}{2\mathscr{E}_0}+e^2n_e^{1/3}$$
$$\approx 3\cdot10^{-7}-1\cdot10^{-4}\ \text{eV}. \tag{1.26}$$

Postponing the discussion of the nature of this flattened distribution to Secs. 4.1 and 4.2, let us consider its effect on the efficiency of electron cooling. In this case it is possible to distinguish the three characteristic regions of high, low, and superlow velocities of the cooled particle (Fig. 3):

$\Delta_\perp<V$—high velocity (H=High),

$\Delta_\parallel<V<\Delta_\perp$—low velocity (L=Low),

$V<\Delta_\parallel$—superlow velocity (S=Superlow). (1.27)

In the first region, that of high velocities, the cooling dynamics is essentially the same as that in the case of an isotropic Maxwellian distribution, which follows directly from the Coulomb analogy: the field of a "charged ellipse" coincides at large distances with the field of a point charge.

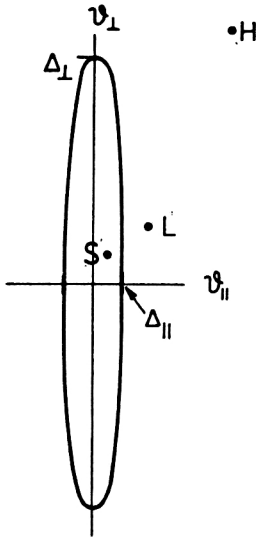

FIG. 3. Flattened electron velocity distribution. The line of constant density labeled H, L, S is the position of the particle in velocity space for the three cases in (1.27).

Accordingly, the friction force and the diffusion power are described by the same expressions as in the case of an isotropic distribution for $\nu_p \gg \Delta_e$ [see Eqs. (1.9), (1.18), and (1.20)]. The power of the friction force here is considerably greater than the diffusion power $[P \approx -(M/m)Q]$, and the particle is cooled, losing its velocity until it falls into the second region of low velocities.

In this region the friction force is the analog of the Coulomb force of a charged disk (a layer) near its axis. Taking into account (1.8) and (1.26), for the longitudinal component we find

$$\vec{F}_\parallel = \frac{\vec{V}_\parallel}{V_\parallel} 2\pi \int_{-\infty}^{\infty} \rho_{\text{equ}}(v_\parallel, 0) dv_\parallel = -\frac{\vec{V}_\parallel}{V_\parallel} \frac{2qL_C}{m\Delta_\perp^2}.$$

To estimate the transverse component we can use the same Coulomb analogy: outside the disk, where there is no charge, we have

$$\text{div}\, \vec{F} = 0,$$

from which

$$F_\perp \approx \frac{V_\perp}{2}\left(-\frac{\partial F_\parallel}{\partial F_\parallel}\right) \approx -V_\perp \frac{F_\parallel}{\Delta_\perp},$$

which gives

$$F_\perp = -V_\perp \frac{4\pi q L_C}{m\Delta_\perp^3}.$$

The coefficients of the diffusion tensor in the region of low velocities can be obtained by substituting (1.26) into (1.11) and integrating (taking into account the axial symmetry). The results are given below [see (1.28)].

In the region of *superlow velocities* the particle falls outside the "disk," where the friction force has only a longitudinal component (again, the Coulomb analogy):

$$\vec{F}_\parallel \approx \frac{\vec{V}_\parallel}{V_\parallel} 2\pi \int_{-V_\parallel}^{V_\parallel} \rho_{\text{equ}}(0) \cdot dv_\parallel \approx -\vec{V}_\parallel \frac{4\pi q L_C}{m\Delta_\perp^2 \Delta_\parallel}.$$

Diffusion in this region is determined, as in the preceding case, by the "hot" transverse component of the electron velocity, since the expression for the diffusion power in the two regions is the same.

Summing these results, we can write down the friction force and the power in an electron beam with the flattened distribution (1.26):

$$\vec{F}_\perp = -\vec{V}_\perp \frac{4\pi q L_C}{m} \times \begin{cases} 1/V^3; \\ 1/\Delta_\perp^3; \\ 0; \end{cases}$$

$$\vec{F}_\parallel = -\vec{V}_\parallel \frac{4\pi q L_C}{m} \times \begin{cases} 1/V^3; & V > \Delta_\perp; \\ 1/V_\parallel \Delta_\perp^2; & \Delta_\parallel < V < \Delta_\perp; \\ 1/\Delta_\parallel \Delta_\perp^2; & V < \Delta_\parallel; \end{cases}$$

$$Q_\perp = Q_\parallel = \frac{4\pi q L_C}{m} \times \begin{cases} 1/V, & V > \Delta_\perp; \\ 1/\Delta_\perp, & V < \Delta_\perp. \end{cases} \tag{1.28}$$

It is more convenient to discuss the features of the cooling process arising from the flatness of the electron distribution function in the next subsection. Here we confine ourselves to writing out the expression for the equilibrium value of the velocity of a cooled particle, substituting (1.28) into the Langevin equation (1.14):

$$\sqrt{(\overline{V_\perp^2})_{\text{equ}}} = \sqrt{\frac{m}{M}}\,\Delta_\perp, \quad \sqrt{(\overline{V_\parallel^2})_{\text{equ}}} = \sqrt{\frac{m}{M}\Delta_\perp \Delta_\parallel}. \tag{1.29}$$

1.4. A magnetized electron beam

If the electron beam is located in a magnetic field parallel to the beam axis and accompanying it from the cathode of the electron gun to the collector, the electron trajectories in the lab frame are spirals with radius $\rho_\perp$ and pitch λ_B wrapped around the magnetic field lines (in the particle frame the pitch of the spiral is obviously smaller by a factor of $v_\parallel / v_0$):

$$\rho_\perp = \frac{v_\perp}{\omega_B}, \quad \lambda_B = v_0 T_B, \quad \omega_B = \frac{eB}{\gamma m c} = \frac{2\pi}{T_B},$$

$$\gamma = \left(1 - \frac{v_0^2}{c^2}\right)^{-1/2}. \tag{1.30}$$

For a sufficiently strong magnetic field an electron in a collision with a particle cannot be displaced in the direction perpendicular to the magnetic field, and this considerably changes the picture of the collision: instead of the classical two-body problem we have the problem of a collision with a bound electron. As a result, the "mass" of the body receiving the impact is sharply increased. In addition, a sharp anisotropy appears in this mass: the electron is freely displaced along the field and weakly displaced in the direction transverse to it. In the limiting case of complete magnetization, i.e., an infinitely strong magnetic field, the electron is similar to a bead on an abacus, which moves freely only along a

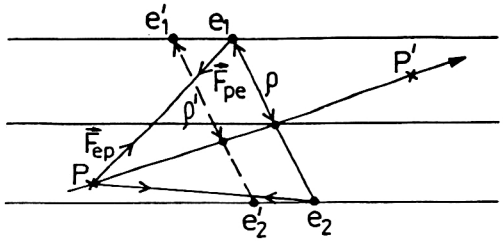

FIG. 4. Change of the impact parameter in a collision of a particle with magnetized electrons: the case of coplanar trajectories of the particle (pp') and the electron (ee').

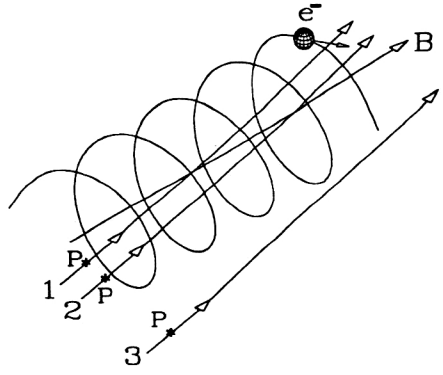

FIG. 5. Three types of collisions between a particle and an electron in a magnetic field: fast (*1*), adiabatic (*2*), and "magnetized" (*3*).

spoke—the field line. During a collision with a particle the electron moves, and the impact parameter ρ is changed in the course of the collision (Fig. 4). Accordingly, the interaction between the particle and the electron becomes stronger or weaker, depending on the sign of $\Delta\rho$. The result summed over all possible collisions gives (Refs. 10, 23, and 24) a decelerating force directed, in general, opposite to the particle velocity $\vec{V}$:

$$\vec{F}_\perp = -\vec{V}_\perp \cdot \frac{2\pi q L_C}{mV^3}\frac{V_\perp^2 - 2V_\parallel^2}{V^2},$$

$$\vec{F}_\parallel = -\vec{V}_\parallel \frac{2\pi q}{mV^3}\left(\frac{3V_\perp^2}{V^2}L_C + 2\right), \quad L_C = \ln\frac{\rho_{\max}}{\rho_{\min}}. \qquad (1.31)$$

An important difference between the equations for the friction force (1.16) and (1.28) and Eq. (1.31) should be noted. Here $F_\perp$ changes sign (deceleration changes to acceleration) when $V_\perp < \sqrt{2}V_\parallel$, and the first term in parentheses for $F_\parallel$ vanishes for $V_\perp \to 0$. This behavior of the friction force is explained[10,20] by the abacus-bead-like behavior of the interaction of the particle with a magnetized electron discussed above. This is seen especially clearly in the case of $F_\parallel$: if $V_\perp \to 0$, the particle moves strictly along a field line and the total momentum transfer is zero for $\rho \leq \rho_{\max}$. The term in parentheses without the logarithm directly takes into account the contribution of larger impact parameters.

The Coulomb logarithm L_C deserves special discussion. Since the electron motion perpendicular to the field lines is "frozen," the electron cloud can respond to the effect of the electric field of the particle only by longitudinal displacement of the electrons. Therefore, the Debye screening length, which is defined relative to the particle velocity, is in this case equal to

$$R_D = \frac{U_M}{\omega_{pe}}\begin{cases} V/\omega_{pe} \approx 0.05 \text{ cm}, & V > \Delta_\parallel, \\ \Delta_\parallel/\omega_{pe} \approx 5\cdot 10^{-4} \text{ cm}, & V < \Delta_\parallel, \end{cases}$$

$$U_M = \langle|\vec{V} - \Delta_\parallel|\rangle, \qquad (1.32)$$

where ω_{pe} is the electron plasma frequency (1.5). However, the formal use of the expression for the Debye length becomes meaningless at low electron density and small $\Delta_\parallel$, when the Debye sphere is "empty." Therefore, at superlow particle velocities it is reasonable to take as $\rho_{\max}$ the radius of a sphere containing a sufficiently large number of electrons k:

$$R_e \equiv \left(\frac{k}{n_e}\right)^{1/3}, \quad k \approx 3z.$$

Then the value of $\rho_{\max}$ in collisions of the particle with magnetized electrons can be chosen to be

$$\rho_{\max} = \min\begin{cases} a \approx 1.5 \text{ cm} \\ \max\{R_D, R_e\} \approx 0.1 \text{ cm} \\ U_M \tau \approx 0.5 - 0.05 \text{ cm}. \end{cases} \qquad (1.33)$$

Here, as before, a is the cross-sectional radius of the electron beam and τ is the time for the particle to pass through the cooling system. The value of $\rho_{\min}$ is discussed below [see (1.34)].

In a magnetic field of finite strength there are three ranges of impact parameter (Fig. 5) which are determined by the beam parameters: the electron Larmor radius $\rho_\perp$ (1.30) and the spread of the electron longitudinal velocities $\Delta_\parallel$ (1.26).

(1) *Small impact parameters.* The particle interacts with the electron so rapidly that the magnetic field has no effect on the electron motion. This happens if the collision time is much smaller than the Larmor (cyclotron) period of rotation of the electron T_B:

$$\tau_{\text{col}} \approx \rho/U_M \ll T_B.$$

Such collisions are termed fast (subscript F for fast), and for them the impact parameter lies in the range

$$\rho_{\min} \leq \rho \leq \rho_F,$$

$$\rho_{\min} = \frac{ze^2}{mU^2} = \frac{ze^2}{m}\begin{cases} V^{-2}; \\ \Delta_\perp^2; \end{cases}$$

$$\rho_F \simeq \frac{U_M}{\omega_B} \approx \begin{cases} V/\omega_B, & V > \Delta_\parallel; \\ \Delta_\parallel/\omega_B, & V < \Delta_\parallel; \end{cases}$$

$$U = \langle|\vec{V} - \vec{\Delta}_\perp|\rangle. \qquad (1.34)$$

The friction force and the diffusion for fast collisions are described by the expressions for the flattened distribution (1.28) with the substitution $\rho_{\max} = \rho_F$.

(2) *Intermediate impact parameters* $\rho_F \leq \rho \leq 2\langle\rho_\perp\rangle$. [We note that the factor of two in the upper limit was chosen on the basis of considerations regarding the smoothness of the

function $\vec{F}(\vec{V})$; see Eqs. (1.36) and (1.37) and the discussion below.] In collisions with these impact parameters the particle and the electron move together for several periods of the cyclotron revolution of the electron, when the electron revolves "around" the particle, colliding with it several times:

$$N_{\text{col}} \approx 1 + \frac{\tau_{\text{col}}}{T_B} \leqslant 1 + \frac{2\langle \rho_\perp \rangle}{U_M T_B}.$$

Taking into account (1.30), this gives

$$1 \leqslant N_{\text{col}} \leqslant 1 + \left[\frac{\Delta_\perp}{\pi U_M}\right] \approx 1 + \begin{cases} N_L = \left[\dfrac{\Delta_\perp}{\pi V}\right], & V > \Delta_\parallel, \\ N_S = \left[\dfrac{\Delta_\perp}{\pi \Delta_\parallel}\right], & V < \Delta_\parallel, \end{cases} \tag{1.35}$$

where [ ] denotes the integral part.

The friction force and the diffusion in adiabatic collisions are N_{col} times larger than for the free electron (1.28).

(3) *Large impact parameters* $2\langle \rho_\perp \rangle \leqslant \rho \leqslant \rho_{\max}$. Here the electron appears to be a Larmor disk and the collisions have the same character as for magnetized electrons (1.31).

It follows from Eqs. (1.32) and (1.34) that the choice of value of the impact parameter depends primarily on the particle velocity. As before, we can distinguish three characteristic ranges of V (1.27).

At large velocity only two types of collision contribute to the friction force: fast and magnetized ones. Adiabatic collisions are absent, since for $V > \Delta_\perp$ the number of collisions is $N_{\text{col}} = 1$.

At low and superlow velocities three types of collision are possible, and the friction force contains three terms, respectively, taking into account the contributions of fast, adiabatic, and magnetized collisions. Here magnetized collisions at superlow velocities require additional analysis, since it is no longer possible to neglect $\Delta_\parallel$.

It is convenient to estimate the momentum transferred to a particle in such a collision by going to the particle frame, where the electrons have velocities

$$\vec{v}' \approx -\vec{V} + \vec{v}'_\parallel .$$

The momentum transfer can then be split into two components, along and perpendicular to the vector $\vec{v}$. Only the longitudinal component contributes to the force, as the transverse one is of higher order in smallness. The first, Δp_v, is equal to the integral of the force of attraction along trajectory AA of the electron in the particle frame (Fig. 6), taking into account the change of the electron velocity Δv:

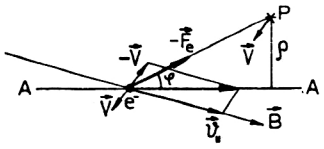

FIG. 6. Scheme for particle collision with a magnetized electron: P is the particle, AA is the electron trajectory, and $\vec{B}$ is the magnetic field line of force.

$$\Delta p_v \approx \int_{-l}^{0} (-F_e)\cos\varphi \frac{ds}{v'} - \int_{0}^{l} (-F_e)\frac{ds}{v' + \Delta v'},$$

$$F_e = \frac{ze^2}{\rho^2 + s^2}, \quad \Delta v' \approx \frac{1}{m}\int_{-l}^{0} F_e \cos\varphi \frac{ds}{v'} \approx \frac{ze^2}{m\rho\Delta_\parallel},$$

where $2l$ is the typical interaction length, s is the coordinate along the trajectory, and ρ is the impact parameter. Integration along the trajectory gives

$$\Delta p_v \approx \left(\frac{ze^2}{\rho}\right)^2 \frac{1}{m(v')^3},$$

and integration over all possible collisions leads to the expression for the force. Since $\langle \vec{v} \rangle = V$, we obtain

$$\vec{F}_v = n_e \int_v^\rho \int_{\rho_{\min}}^{\rho_{\max}} \vec{v} f(\vec{v}) d^3v \Delta p_v 2\pi\rho d\rho \approx -\vec{V}\frac{2\pi q}{m\Delta_\parallel^3} L_{MS},$$

$$L_{MS} = \ln \frac{\rho_{\max}}{\langle \rho_\perp \rangle}.$$

Here L_{MS} is the Coulomb logarithm for collisions with magnetized electrons at superlow particle velocities, and $\rho_{\max}$ is given in Eq. (1.33). This result differs from the exact one[10] by the factor $\sqrt{2/\pi}$.

Now we can write down the full expression for the friction force in the electron beam at finite magnetic field strength for three ranges of the particle velocity:[25]

$$\vec{F}_\perp \approx -\frac{2\pi q}{m}\vec{V}_\perp \times \begin{cases} \dfrac{1}{V^3}\left(2L_{FH} + \dfrac{V_\perp^2 - 2V_\parallel^2}{V^2} L_{MH}\right), & \text{H} \\ \dfrac{2}{\Delta_\perp^3}(L_{FL} + N_L L_{AL}) + \dfrac{V_\perp^2 - 2V_\parallel^2}{V^2}\dfrac{L_{ML}}{V^3}, & \text{L} \\ \dfrac{2}{\Delta_\perp^3}(L_{FS} + N_S L_{AS}) + \dfrac{L_{MS}}{V^3}, & \text{S} \end{cases}$$

$$\vec{F}_{\parallel}\approx-\frac{2\pi q}{m}\vec{V}_{\parallel}\times\begin{cases}\dfrac{1}{V^3}\left(2L_{FH}+\dfrac{3V_{\perp}^2}{V^2}L_{MH}+2\right), & \text{H}\\ \dfrac{2}{\Delta_{\perp}^2 V_{\parallel}}(L_{FL}+N_L L_{AL})+\left(\dfrac{3V_{\perp}^2}{V^2}L_{ML}+2\right)\dfrac{1}{V^3}, & \text{L}\\ \dfrac{2}{\Delta_{\perp}^2\Delta_{\parallel}}(L_{FS}+N_S L_{AS})+\dfrac{L_{MS}}{\Delta_{\parallel}^3}, & \text{S.}\end{cases} \tag{1.36}$$

The Coulomb logarithms for each region are the following:

For high particle velocities (H)

$$L_{MH}=\ln\frac{(\rho_{\max})_H}{2\langle\rho_{\perp}\rangle}\approx\ln\frac{V\omega_B}{2\Delta_{\perp}\omega_{pe}}\approx 2;$$

$$L_{FH}=\ln\frac{\rho_{FH}}{(\rho_{\min})_{\parallel}}\approx\ln\frac{mV^3}{ze^2\omega_B}\approx 10-\ln z.$$

For low particle velocities (L)

$$L_{ML}=\ln\left[\frac{(\rho_{\max})_L}{2\langle\rho_{\perp}\rangle}\right]\approx\ln\left[\frac{\min\{(V/\omega_{pe}),(3z/n_e)^{1/3}\}}{2\langle\rho_{\perp}\rangle}\right]\approx 3-1;$$

$$L_{AL}=\ln\left[\frac{2\langle\rho_{\perp}\rangle}{\rho_{FL}}\right]\approx\ln\left[\frac{2\Delta_{\perp}}{(\Delta_{\perp}\to\Delta_{\parallel})}\right]\approx 0.7\to 4; \tag{1.37}$$

$$L_{FL}=\ln\left[\frac{\rho_{FL}}{(\rho_{\min})_L}\right]\approx\ln\left[\frac{mV^3}{ze^2\omega_B}\right]\approx 5-\ln z.$$

For superlow particle velocities (S)

$$L_{MS}=\ln\left[\frac{(\rho_{\max})_S}{\langle\rho_{\perp}\rangle}\right]\approx\ln\left[\frac{1}{2\langle\rho_{\perp}\rangle}\left(\frac{3z}{n_e}\right)^{1/3}\right]\approx 2;$$

$$L_{AS}=\ln\left[\frac{2\langle\rho_{\perp}\rangle}{\rho_{FS}}\right]\approx\ln\frac{2\Delta_{\perp}}{\Delta_{\parallel}}\approx 5;$$

$$L_{FS}=\ln\left[\frac{\rho_{FS}}{(\rho_{\min})_S}\right]\approx\ln\left[\frac{m\Delta_{\parallel}\Delta_{\perp}^2}{ze^2\omega_B}\right]\approx 5-\ln z. \tag{1.37c}$$

This collection of Coulomb logarithms shows how complicated the dependence of the friction force on the parameters is.

Before discussing the general behavior of the function $\vec{F}(\vec{V})$, let us note some of its features.

First, the function is practically continuous at the point $|\vec{V}|=\Delta_{\perp}$. The factor of two was introduced into the boundary value of the impact parameter $2\langle\rho_{\perp}\rangle$ for smoothing. Although this was done quite arbitrarily, the logarithmic dependence reduces the severity of the problem.

Equations (1.36) and (1.37) also require a definite accuracy at large and small values of the magnetic field, where their formal use gives a physically meaningless result: the Coulomb logarithms tend to infinity (+ or −) if $B\to 0$ or ∞. Physically, this means that for $\rho_{\perp}>\rho_{\max}$ there are no magnetized collisions at all and L_M must be set equal to zero, while for $\rho_{\perp}>\rho_F$ adiabatic collisions disappear and L_A must be zero. Finally, if $\rho_{\perp}<\rho_{\min}$, in L_M it is necessary to use $\rho_{\min}$ (the "absolute" magnetization) instead of $\rho_{\perp}$.

Therefore, the magnetization of the electrons begins to be felt when

$$2\langle\rho_{\perp}\rangle<(\rho_{\max})_L, \quad \text{or} \quad B\geq\frac{2mc}{e}\omega_{pe}\approx 120\ \text{G}.$$

This condition is, of course, weak, and already at $V\approx 0.5\Delta_{\perp}$ this magnetization is not noticeable. The magnetization can be assumed "complete" if it is manifested right down to superlow velocities, when the third term $L_{MS}/\Delta_{\parallel}^3$ contributes in the expression for the friction force. This occurs if

$$\langle\rho_{\perp}\rangle<(\rho_{\max})_S, \quad \text{or} \quad B\geq\frac{m\Delta_{\perp}c}{e}\left(\frac{n_e}{3z}\right)^{1/3}\approx\frac{800}{z^{1/3}}\ \text{G}. \tag{1.38}$$

"Absolute" magnetization sets in when

$$\langle\rho_{\perp}\rangle\leq(\rho_{\min})_S, \quad \text{or} \quad B\geq\frac{m^2\Delta_{\perp}^3 c}{ze^3}\approx 6\ \text{MG},$$

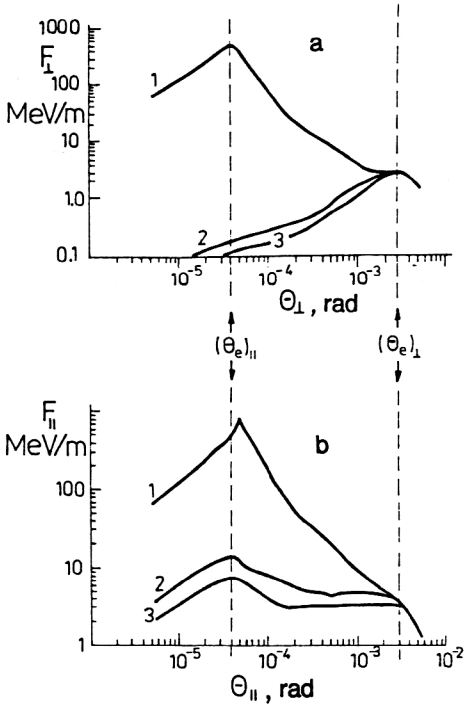

FIG. 7. Dependence of the transverse (a) and longitudinal (b) components of the friction force (1.37) on the particle velocity: $(\theta_p)_{\perp,\parallel}=V_{\perp,\parallel}/v_0$ for an electron beam with flattened distribution and parameters in Table III. $B=3$ kG (1), 0.6 kG (2), and 0.1 kG (3). In case (a) $V_{\parallel}=0$, and in case (b) $V_{\perp}=0$.

which is not very realistic. It is important that the magnetization criterion (1.38) contains the electron density.

It is natural to incorporate this logic into a program for numerical computations. An example of such a calculation is shown in Fig. 7. Here the approximate nature of Eqs. (1.36) and (1.37)—the nonmonotonicity of the friction force in the case of moderate magnetization (curves 2) is especially clear. It should be noted that for an unmagnetized beam (curves *3*) $F_\perp$ reaches a maximum for $V=\Delta_\perp$, while $F_\parallel$ reaches one for $V=\Delta_\parallel$.

The second fact worth noting is the increase of the friction force with decreasing particle velocity at low velocities up to $V\approx\Delta_\parallel$ (Fig. 7, curves *1*). This effect, which distinguishes a magnetized beam from an unmagnetized one [compare (1.36) with (1.28) and (1.9)], also explains the phenomenon of "fast" electron cooling, described in the Introduction.

The friction force in a magnetized beam reaches a maximum for $V\approx\Delta_\parallel$. In this region the approximation of binary particle–electron collisions already works poorly (see Sec. 5). Nevertheless, from (1.36) we find

$$F_{\max}\sim-\frac{2\pi q}{\Delta_\parallel^2}L_{MS}\sim-2\pi z^2e^2n_e^{2/3}. \tag{1.39}$$

The last expression is obtained if the value of $\Delta_\parallel$ from (1.26) or from (4.5) and (4.6) below is used and we take $L_{MS}\sim1$. The question of the power of z remains open (Sec. 5). On the other hand, $F_{\max}$ (1.39) is equal in order of magnitude to the force acting on a point charge ze by the same electron charge located at a distance $l_e=n_e^{-1/3}$ from it.

Finally, the third feature of the friction force is the great difference between its transverse and longitudinal components at low velocities. This is caused by the flattened distribution: the axial component of the field of a charged disk (Fig. 3) close to its surface is much larger than the radial component. As a result, the longitudinal component of the particle velocity is cooled in the region $V<\Delta_\perp$ more quickly than the transverse component. The ratio $F_\parallel/F_\perp$ is of the order of $\Delta_\perp/V_\parallel$ for $V\sim\Delta_\perp$ and of order 3 for $\Delta_\perp\gg V>\Delta_\parallel$.

The diffusion is noticeable only at superlow velocities, where it determines the equilibrium state of the cooled beam. It can be estimated by using the same scheme as in deriving Δp_v (Fig. 6). After calculating the radial component of the momentum transfer

$$\Delta p_\perp=\int_{-l}^{l}(-F_e)\sin\varphi\,\frac{ds}{v}\approx\frac{2ze^2}{\rho v_e},$$

we find the mean-square momentum transferred per unit time:

$$\frac{d\overline{\Delta p^2}}{dt}\approx n_e\Delta_\parallel\int_{(\rho_{\min})_S}^{(\rho_{\max})_S}(\Delta p_\perp)^2 2\pi\rho d\rho,$$

from which

$$Q\approx\frac{4\pi q}{M\Delta_\parallel}L_{MS}. \tag{1.40}$$

This result differs from the exact one[10] by the factor $\sqrt{\pi/2}\ln(\Delta_\parallel/\Delta_\perp)\approx1$.

Substitution of the expressions for the force (1.36) and for the diffusion power (1.40) at superlow velocities into the Langevin equation (1.14) gives the equilibrium value of the temperature and velocity of a particle cooled in a magnetized beam:

$$T_p=T_\parallel,$$
$$\sqrt{\overline{V_{\text{equ}}^2}}\approx\sqrt{\frac{m}{M}}\,\Delta_\parallel. \tag{1.41}$$

In contrast to the case of the nonmagnetized beam (1.29), here all three components of the particle velocity are cooled equally deeply, and the final value of this velocity is determined by the longitudinal spread of electron velocities.

2. HEAVY-PARTICLE BEAMS IN A COOLER

2.1. Betatron oscillations and the cooling time

The motion of particles in the magnetic focusing system of a storage ring introduces certain features into the dynamics of electron cooling. Betatron oscillations cause the instantaneous values of the transverse components of the particle velocity to take all possible values, from zero to the maximum, on the cooling section. The instantaneous value of the friction force is also changed accordingly. Therefore, to calculate the cooling time it is necessary to average over the betatron oscillations.[20]

Let us restrict ourselves to the case of a beam freely circulating in the constant field of a storage ring (the accelerating high-frequency voltage is switched off). The particle undergoes betatron oscillations around some closed orbit whose position in space is determined by the deviation of the longitudinal component of the momentum from the equilibrium value:

$$\Delta x(s)=\psi(s)\frac{\Delta p}{p}, \tag{2.1}$$

where s is the longitudinal coordinate and $\psi(s)$ is the dispersion function of the storage ring. In the process of cooling Δp and, accordingly, Δx fall off sufficiently slowly, so that

$$\omega_x\frac{d\Delta x}{dt}\ll\Delta x,$$

where ω_x is the frequency of the radial betatron oscillations. Therefore, the radial oscillations, like the vertical ones, can in this case be described by the oscillator equation with weak friction:

$$\ddot{x}+\omega_x^2x=\frac{1}{M}F_x(\vec{V}),$$

$$x(t)=\frac{V_0}{\omega_x}\sin\varphi,\quad \varphi=\omega_xt+\varphi_0.$$

As before, we are considering the particle motion in a moving frame (the electron frame), and the transformation to the lab frame will be discussed below.

Multiplying both sides of the equation by $\dot{x}$ and averaging over the oscillation period, we obtain

$$\frac{dV_0^2}{dt}=\frac{2}{M}\overline{F_x(\vec{V})V_x}=\frac{2}{M}\bar{P}_x.$$

This is none other than the Langevin equation for the oscillator (the diffusion can be neglected at large V_0); here, in contrast to (1.13), V_0 is the amplitude of the velocity. From this the decrement of the damping of the oscillations is

$$\lambda_x\equiv-\frac{1}{V_0^2}\frac{dV_0^2}{dt}=-\frac{2}{MV_0^2}\overline{P_x(\vec{V})}. \tag{2.2}$$

It is sometimes convenient to use a different expression for the decrement. Taking into account the fact that

$$F(\vec{V})\approx\vec{F}(\vec{V}^*)+\left.\frac{\partial F}{\partial V}\right|_{\vec{V}^*=\vec{V}}(\vec{V}^*-\vec{V}),$$

from (2.2) we find the value of the decrement at the point $\vec{V}^*$:

$$\lambda_x=-\frac{2\bar{V}^2}{MV_0^2}\left.\frac{\partial F}{\partial V}\right|_{\vec{V}^*=\vec{V}}.$$

From this it follows, in particular, that for a free particle ($\bar{V}^2=V_0^2$) the decrement is twice as large as for the oscillator ($\bar{V}^2=V_0^2/2$). This fact must be taken into account in calculating the decrements for the longitudinal (free) and transverse (betatron oscillations) degrees of freedom. The same relations hold for the z oscillations. To avoid confusion, we stress that (2.2) is the decrement of the damping of the squared amplitude or the squared velocity (i.e., the beam emittance), while the decrement for the amplitude or the velocity is half that. This nearly trivial observation is often forgotten when experimental results are analyzed.

The situation is simplest at superlow velocities, where the friction force is proportional to the particle velocity. For a magnetized electron beam

$$\lambda_x=\lambda_z\approx\frac{2\pi q}{mM}\frac{L_{MS}}{\Delta_\parallel^3}. \tag{2.3}$$

At high and low velocities the complicated dependence of the friction force on the velocity does not permit such simple averaging. It is possible only to make rather rough estimates, neglecting the dependence of the Coulomb logarithms on the particle velocity [see (1.37)]. Then for a completely magnetized electron beam we can take

$$\vec{F}\approx-\frac{4\pi q}{m}\vec{V}\frac{L_C}{V^3},\quad L_C\approx 10,\quad V>\Delta_\parallel. \tag{2.4}$$

Now two cases important in practice can be distinguished:

(a) Strictly one-dimensional oscillations, except that they are in one of the transverse degrees of freedom; this situation is typical in experiments to measure the cooling time (see Sec. 3 below).

(b) Oscillations in all three degrees of freedom are excited; this occurs, for example, in the storage of heavy particles in a cooler.

In case (a) we have

$$V_x\approx\begin{cases}V_0\cos\varphi, & V_x>\Delta_\parallel\\ \Delta_\parallel, & V_x<\Delta_\parallel,\end{cases}$$

which gives

$$\bar{P}_x\approx-\frac{4\pi qL_C}{m}\frac{1}{\tau}\int_0^{\tau\to\infty}\frac{V_x^2dt}{V^3}$$

$$\approx-\frac{4\pi qL_C}{mV_0}\frac{2}{\pi}\left(\int_0^{\pi/2-\delta}\frac{d\varphi}{\cos\varphi}+\frac{V_0^3}{\Delta_\parallel^3}\int_{\pi/2-\delta}^{\pi/2}\cos^2\varphi d\varphi\right),$$

where $\delta=\Delta_\parallel/V_0\ll 1$. Performing the integration, after substitution into (2.2) we find

$$\lambda_x\approx\frac{16qL_C}{mMV_0^3}\ln\frac{V_0}{\Delta_\parallel}. \tag{2.5}$$

The total cooling time for "large amplitudes" is obtained by integrating (2.2), taking into account (2.5):

$$\tau_\alpha\approx\frac{mM}{24qL_C}\frac{V_0^3}{\ln(V_0/\Delta_\parallel)}. \tag{2.6}$$

Therefore, compared with the result (1.13) and (2.4) for free particles, the cooling time in case (a) is decreased by a factor of $(2/\pi)\ln(V_0/\Delta_\parallel)$.

In case (b) the effect of betatron oscillations is not so important, because the transverse components of the velocity change with opposite phases, and the longitudinal component changes monotonically. Therefore, in the denominator of (2.4) we can set $V\approx V_0$ and write

$$\bar{P}_x\approx-\frac{2\pi qL_C}{mV_0},$$

which gives, as in (2.5) and (2.6),

$$\tau_b\approx\frac{mMV_0^3}{6\pi qL_C}. \tag{2.7}$$

We also stress that this is the cooling time of the squared amplitude of the velocity, i.e., the emittance of the particle beam.

2.2. The cooling time in the lab frame

Equations (2.6) and (2.7) were obtained in the electron frame. To transform to the lab frame it is necessary to include the Lorentz factor γ in the transformation of the time and the electron density. In addition, it is convenient to express the electron density in terms of the current density of the electron beam averaged over the particle orbit:

$$\langle n_e\rangle=\frac{\eta J}{e\gamma\beta c},\quad \eta=\frac{l_{\text{cool}}}{C};\quad J=\frac{I}{\pi a_{\max}^2},$$

$$a_{\max}=\max\{a_e,a_p\}, \tag{2.8}$$

where a_e and a_p are the cross-sectional radii of the two beams on the cooling section of length l_{cool}, C is the perimeter of the storage ring, and I is the electron current. It is also convenient to introduce the parameter

$$\theta=\frac{\Delta p_\alpha}{p_0},$$

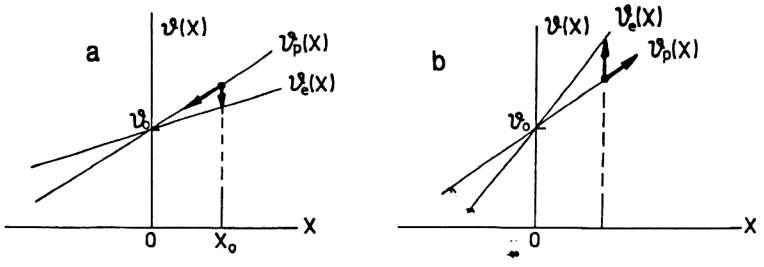

FIG. 8. Effect of cooling in an electron beam with linear gradient of the velocity along the radius: (a) stable regime, particles "roll down" to the beam axis; (b) unstable regime, particles "escape" from the beam.

where Δp_α is the deviation of the component of the particle momentum ($\alpha = x,z,s$) from the equilibrium value p_0 in the lab frame. Obviously,

$$\theta_{x,z} = \frac{\Delta p_{x,z}}{p_0} = \frac{V_{x,z}}{\gamma\beta c}, \quad \beta = \frac{v_0}{c}, \quad \gamma = (1-\beta^2)^{-1/2},$$

$$\theta_e = \frac{\Delta_\perp}{\gamma\beta c}, \quad \theta_s = \frac{\Delta p_s}{p_0} = \frac{V_\parallel}{\beta c},$$

$$\theta_\parallel = \frac{\Delta_\parallel}{\beta c}, \quad \varepsilon_{x,z} = \beta_{x,z}\theta_{x,z}^2, \tag{2.9}$$

where ε is the beam emittance and $\beta_{x,z}$ are the so-called betatron functions of the storage ring. In this notation Eqs. (2.6) and (2.7) take the form

$$\tau_{\text{lab}} \approx \frac{\beta^4\gamma^2}{6kcr_pL_C}\frac{mc^3}{\eta eJ}\frac{A}{z^2} \times \begin{cases} \gamma^3\theta_{x,z}^3 & \text{for the } x,z \text{ components,} \\ \theta_\parallel^3 & \text{for the } s \text{ component,} \end{cases} \tag{2.10}$$

where $r_p = 1.534\times10^{-16}$ cm is the classical proton radius, A and ze are the atomic weight and charge of the particle (we also note that $mc^3/e = 17kA$), and

$$k = \begin{cases} \pi & \text{for three-dimensional oscillations,} \\ 4\ln(\theta_{x,z}/\theta_\parallel) & \text{for one-dimensional oscillations} \\ & \text{in } x \text{ or } z. \end{cases}$$

For typical parameters (Table III) Eq. (2.10) gives $\tau_{\text{lab}} = 2.9$ sec in the case of three-dimensional oscillations, while numerical integration of (1.36) gives 2.85 sec. The closeness of these results reflects the fact that three-dimensional oscillations from the viewpoint of the cooling dynamics (the particle velocity does not vanish) are close to the case of a free particle.

2.3. Monochromatic instability

When the electron beam is aligned relative to the equilibrium particle trajectory at some angle α, a so-called monochromatic instability can arise.[10,20] Such an alignment is equivalent to the appearance in the electron beam of a constant transverse velocity $\Delta v_\perp = \gamma\beta c\alpha$ (in the electron frame). In undergoing betatron oscillations the particle moves either along or opposite to this velocity. Since the relative velocity of the particle and the electrons in the first case is much smaller (the difference of the velocities) than in the second (the sum), the friction force causes the oscillations to grow to an amplitude $V_0 \approx \Delta v_\perp$. The velocity of the "cooled" beam significantly exceeds the limit (1.41). The critical value of the angle α_0 at which this instability develops depends on the parameters of the cooling system. If the beam is not magnetized, the critical angle is determined by the spread in the transverse velocities: $\Delta v_\perp > \Delta_\perp$, $\alpha > \theta_e$. In a magnetized electron beam the determining factor is the spread in longitudinal velocities: $\Delta v_\perp > \Delta_\parallel$, $\alpha > \theta_\parallel$. It is true that in this case the final value of the velocity amplitude is also correspondingly smaller, $V_0 \approx \Delta_\parallel$, but it still significantly exceeds the limit (1.41).

The requirements on the uniformity of the magnetic field are no less strict. If, for example, the angle between a line of force and the equilibrium trajectory oscillates with amplitude α_0, this is equivalent to increasing the electron transverse velocity to $\alpha_0\gamma\beta c$. This "heating" of the electron beam does not significantly change the picture of the interaction[10] if

$$\alpha_0 \ll \theta_e. \tag{2.11}$$

2.4. The gradient of the electron velocities

The space charge of the electron beam creates an electron velocity gradient which, in general, lowers the efficiency of electron cooling.[26] Let us explain this effect first for the example of a constant gradient (Fig. 8).

Since electron cooling "tunes" the particle velocities to the average electron velocity, the location of the instantaneous equilibrium orbit about which a particle oscillates in a freely circulating beam is shifted in space (the point x_0 in Fig. 8). This shift is directed inward, toward the axis of the electron beam, or outward, depending on the value of the gradient dv_e/dx. In the first case the beam contracts when cooled, and in the second it expands and goes out of the electron beam. The stability criterion for electron cooling using (2.1) can be written as

$$\frac{dv_e}{dx} \leqslant \frac{dv_p}{dx} = \frac{\beta c}{\gamma^2\psi},$$

where v_p and v_e are the electron and particle velocities in the lab frame, or

$$\frac{\gamma^2\psi}{\beta c}\frac{dv_e}{dx} \leqslant 1. \tag{2.12}$$

In a real cooling system the electron velocities depend nonlinearly on the coordinates. In particular, if the beam density is constant,

$$\frac{dv_e}{dx} = \frac{2eI}{\beta^2c^2\gamma^3m}\frac{x}{a^2}.$$

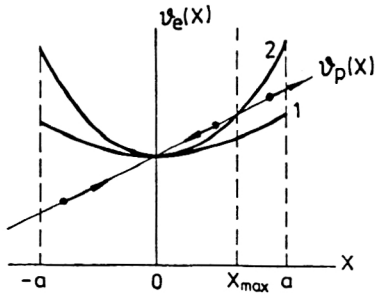

FIG. 9. Distribution of electron velocities in a beam of constant density: (*1*) $I<I_{crit}$; (*2*) $I>I_{crit}$. The particles in the region $x>x_{max}$ leave the beam.

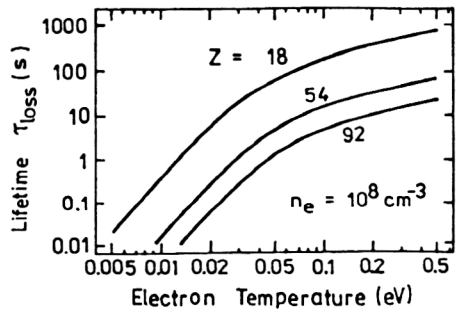

FIG. 10. Electron–ion recombination. Calculated dependence of the lifetime of multiply charged ions on the ion temperature (Ref. 29): $\eta=0.02$, $n_e=10^8$ cm^{-3}. At relativistic energies τ must be multiplied by γ^2.

From this we find a limit on the beam current:

$$I\leqslant\beta^3\gamma\frac{mc^3}{e}\frac{a}{2\psi}\simeq 1\text{ A}. \tag{2.13}$$

If the conditions (2.12) and (2.13) are not satisfied, part of the beam is lost (Fig. 9). Analysis of the effect of the electron velocity gradient on the friction force[20] leads to the same condition (2.12).

2.5. The lifetime of a particle in a cooler

For a beam of moderate intensity far from the development of collective processes making the electron beam unstable, the processes which limit the lifetime of the beam particles are single scattering on the atoms of the residual gas and of the internal target and recombination (for ions) with cooling electrons. As a rule, the effect of multiple scattering is suppressed by electron cooling (Sec. 7.2). The maximum angle of single scattering is determined by the acceptance of the storage ring, $\pi\varepsilon$, and the value of the betatron function β_ε at the scattering point: $\theta_{max}=\sqrt{\varepsilon/\beta_\varepsilon}$. As a result, the particle lifetime is

$$\tau_\theta=\frac{1}{\langle\sigma n_0\rangle v_0}=\frac{\beta^3\gamma^2}{4\pi z_0^2 r_p^2 c}\left(\frac{A}{z}\right)^2\frac{\varepsilon}{\langle n_0\beta_\varepsilon\rangle}. \tag{2.14}$$

Here A and ze are the atomic weight and charge of the particle, z_0 and n_0 are the atomic number and density of the scatterer, and the symbol $\langle\rangle$ denotes averaging along the particle orbit. For a target with the parameters of Table III and $A/z\approx 2$ the lifetime τ_θ amounts to about $1/z_0^2$ hours, which is a serious limitation for large z. (See also evaluations for Eq. (7.1) and the comments to it.)

As a result of recombination, the ion charge decreases abruptly and, accordingly, the radius of its equilibrium orbit increases, which can lead to loss of the ion on the chamber walls. For cooled particles the recombination rate is mainly determined by the electron temperature. At a temperature of order 0.1 eV and above, radiation recombination, i.e., electron capture by an ion with emission of a photon, dominates.[20,27] The radiation-recombination coefficient is

$$\alpha_r\simeq\frac{20\alpha r_e^2 c^2 z^2}{\Delta_\perp\ln(\alpha cz/\Delta_\perp)}, \tag{2.15}$$

where α is the fine-structure constant. The lifetime owing to this process is

$$\tau_r=\frac{1}{\langle\alpha_r n_e\rangle}\simeq 1.38\cdot 10^7\frac{\beta^2\gamma^3\theta_e\ln(z/137\beta\gamma\theta_e)}{z^2\eta J_{\text{A/cm}^2}}. \tag{2.16}$$

For protons and the parameters of Table III, τ_r amounts to more than 200 h, while for lead ions it is only 6 min. It is also necessary to take into account the fact that the cooled (compressed) particle beam usually interacts with the part of the electron beam at the axis, where the electron transverse velocities are an order of magnitude lower. Taking this into account, the quoted numerical estimate is in good agreement with the experimental results from the NAP-M (Refs. 8 and 28).

As the electron temperature decreases the contribution of dielectric recombination (collision of an ion with two electrons, one of which carries off the excitation energy of the ion which has captured the other electron) becomes more and more important.

The results of the calculations of Ref. 29 are shown in Fig. 10.

3. EXPERIMENTAL STUDIES OF THE FRICTION FORCE

Three stages of experimental research can be distinguished in the development of the electron cooling method:

1974–1984: Experiments at proton storage rings at the NPI in Novosibirsk (Refs. 5, 8, 9, and 28), at CERN (Ref. 11), and at Fermilab (Ref. 12).

1985–1988: Experiments at the Model Solenoid setup at the NPI in Novosibirsk (Refs. 23 and 30).

1988–1994: The startup of operation of antiproton and ion storage rings (Table I) and experiments at them.

A detailed description of the experimental setups can be found in the original studies and reviews (Refs. 3, 9, 27, 31, and 32).

The distinguishing feature of the Novosibirsk experiments (Fig. 1) was the use of several techniques for measuring the transverse dimensions (emittance) of the cooled beam: a magnesium jet, a thin quartz filament scatterer rapidly intersecting the beam (Fig. 11), and a detector of the neutral hydrogen atoms formed on the cooling segment. As

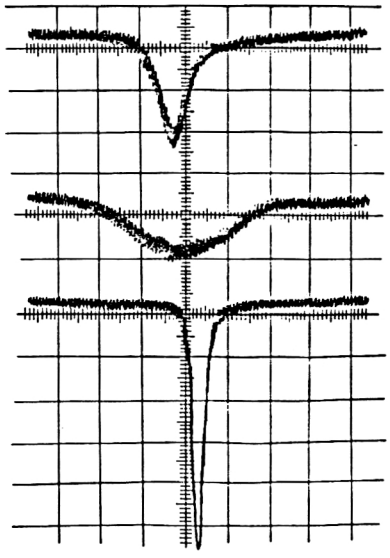

FIG. 11. Beam profile measured by the method of proton scattering by a quartz filament. From top to bottom: the beam immediately after acceleration, the beam after 200 seconds without cooling, and the beam when cooling has been switched on.

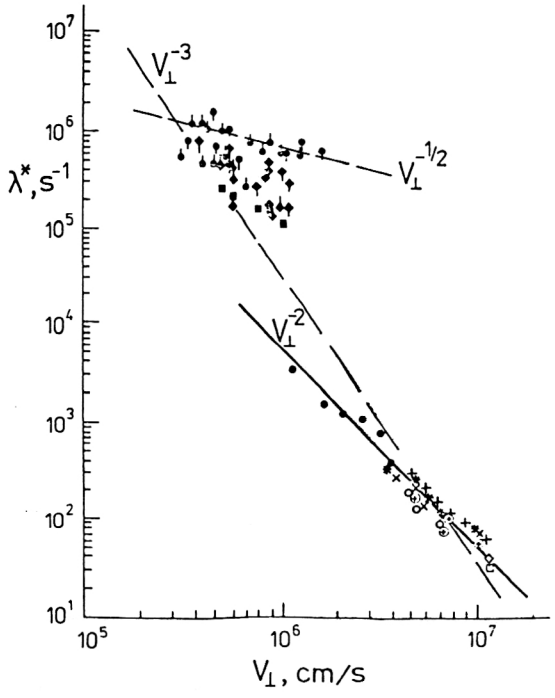

FIG. 12. Dependence of the reduced decrement of damping of transverse oscillations on the relative velocity of the particles and electrons (Refs. 28, 33, and 34):

$$\lambda^* = (A/z^2)\cdot(\lambda_{\exp}/n_e^*), \quad n_e^* = 10^{-8}\eta n_e .$$

Setup	NAP-M (Refs. 3,28), $\lambda_\perp$						TSR (Ref. 33), $\lambda_\parallel$					TSR (Ref. 34), $\lambda_\perp$	
MeV/nucleon	1.5	65	65	65	65	35	12					11.4	
Symbol	•	+	×	⊕	○	*	●	●	◆	◆	■	◆	■
Particles	protons						d	Li^{3+}	C^{6+}	O^{8+}	S^{16+}	C^{6+}	S^{16+}

strange as it may seem, up to now none of the storage rings of the third generation has exploited such technology (only in 1994 was a magnesium jet built in Novosibirsk installed at CELSIUS).

The longitudinal component of the friction force is efficiently measured by using Schottky diagnostics (see Refs. 27 and 32), which make it possible to accurately measure the frequency spectrum of the revolution in the cooled beam. Therefore, in the physics of the electron cooling of ions most of the experimental data have been obtained for the longitudinal degree of freedom.

The measurements of the decrement of the damping of betatron oscillations carried out at the NAP-M accelerator[28] showed (Fig. 12) that for proton energies in the range 1.5–65 MeV the dependence of the decrement on the relative velocity of the particles and the electrons is approximated by the dependence

$$\lambda^* = \frac{A}{z^2}\frac{\lambda_{\exp}}{n_e^*} = \frac{10^6}{(V_\perp^2)_{\text{cm/sec}}} \text{ cm}^3/\text{sec},$$

$$10^6 \leqslant V_\perp \leqslant 10^7 \text{ cm/sec},$$

$$n_e^* = 10^{-8}\eta n_e .$$

Here $\Delta_\perp \approx 2\times 10^7$ cm/sec and $\Delta_\parallel \approx 3\times 10^5$ cm/sec, i.e., the data pertain to low velocities. The measurements of the *longitudinal* friction force and its decrement for multiply charged ions carried out later at the TSR (Ref. 33) for *transverse* velocity in the range 3×10^5 cm/sec $< V_\perp < 10^6$ cm/sec gave curious results (Fig. 12): the two groups of experimental points from the NAP-M ($\lambda_\perp$) and the TSR ($\lambda_\parallel$) lie on the curve $V_\perp^{-3}$ as predicted by the theory (1.36), while the points inside each of the groups follow a weaker dependence, between $V_\perp^{-1/2}$ and $V_\perp^{-2}$. Apparently, more accurate measurements encompassing a wider range of velocities are needed.

The latest TSR results[34] for $\lambda_\perp$ (Fig. 12; C^{6+} and S^{16+} ions) are in good agreement with the NAP-M results.

The properties of the longitudinal component of the friction force have been studied most carefully at the Model Solenoid (MOSOL) setup at the NPI, Novosibirsk (Fig. 13 and Table IV; Ref. 30), where a beam of protons or negatively charged hydrogen ions accelerated in an electrostatic accelerator was cooled during the time of flight through an electron beam. The high time stability of the accelerator energy ensured that the spread of longitudinal velocities of the particles was small, and the use of an H^- source and a magnesium-vapor target which could be switched on remotely made it possible to change the sign of the particle charge while keeping the other parameters fixed. This made very accurate comparison of the values of the friction force for particles of both signs possible. The precision of the experiment was further ensured by the use of a special electrostatic spectrometer (see Ref. 23). Another important feature of the experiment was the high degree of uniformity of the magnetic field.

The results of these experiments and also of most of the others which have been performed by now are shown in Fig. 14 (Refs. 23 and 35–38). They show that at high and low velocities ($V > \Delta_\parallel$) there is good qualitative agreement with the theory. In particular, the magnetization effect is convinc-

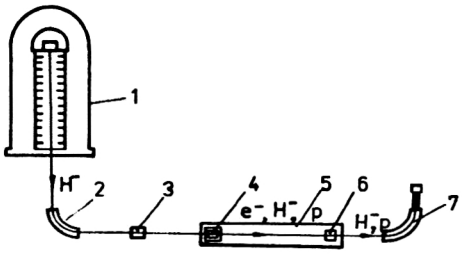

FIG. 13. Schematic diagram of the MOSOL setup: *1*—electrostatic accelerator; *2*—deflector; *3*—magnesium vapor target; *4*—electron gun and plates for beam extraction; *5*—solenoid; *6*—electron collector; *7*—spectrometer.

ingly represented: the friction force continues to grow with decreasing V in the range $V<\Delta_e\approx 3\times 10^7$ cm/sec.

For superlow velocities, four different experiments (MOSOL, IUCF, ESR, and TSR) have revealed a linear dependence of the friction force on $V_\parallel$, as predicted by the theory. However, the absolute value of the force measured experimentally is almost an order of magnitude smaller than that calculated for the density $n_e=1\times 10^8$ cm^{-3} (Fig. 14, left-hand solid line). This difference is apparently related to insufficient stability of the electron energy. Actually, attainment of the maximum level of the friction force at superlow velocities requires the stability

$$\frac{\delta\mathscr{E}}{\mathscr{E}}\ll 2\,\frac{\Delta_\parallel}{\beta c}=2\,\frac{1}{\beta}\,\sqrt{\frac{e^2 n_e^{1/3}}{mc^2}}.$$

The cubic dependence of the force on $\Delta_\parallel$ requires a fairly strong inequality (if only a factor of 3) to eliminate the effect of $\delta\mathscr{E}$. For the MOSOL setup this estimate gives $\delta\mathscr{E}/\mathscr{E}<2\times 10^{-5}$, and for the IUCF and TSR setups it is still an order of magnitude smaller. The correctness of these explanations is also confirmed by the fact that the points of all three experiments lie well on a single curve, which implies the absence of a dependence of the reduced force on the density n_e [we recall that $\Delta_\parallel \propto n_e^{-1/6}$ in the absence of instability of the electron energy; see Eq. (4.5)]. Inhomogeneity of the magnetic field of the electron cooling system has an analogous effect (Sec. 2.3). It is not impossible that the low level of the force in the early experiments at ICE, where also $F_\parallel \propto V_\parallel$ (Fig. 14), was due to the same cause. If this is true, then the pulsations of the electron energy at ICE were about 10^{-3} ($\Delta_\parallel\sim 10^7$ cm/sec).

The cooling of multiply charged ions[33,38] merits special discussion. In the range $V_\parallel>\Delta_\parallel$ good agreement with the theory is observed. At the same time, the experimental data are quite contradictory at superlow velocities: the TSR points coincide well with the points for protons (Fig. 14), but a weak (logarithmic; see Sec. 5.3 and Fig. 17) z dependence is observed. The ESR points[38] lie considerably lower, demonstrating a strong z dependence. The latest results inspire doubt: the values of the reduced friction force for C^{6+} in the ESR experiments lie below the curve for protons and deuterons, while in the TSR experiments they coincide closely with the latter; in addition, the value quoted for Xe^{54+} is larger than that for Ti^{22+}. [We note that in the MOSOL and ESR experiments the curves for $F(V_\parallel)$ were obtained continuously in $V_\parallel$, by scanning the electron energy (MOSOL, Ref.

TABLE IV. Parameters of the MOSOL setup.

Hydrogen ion energy, keV	850
Stability of ion energy, keV	$\pm 2.5\times 10^{-5}$
Electron energy, eV	463
Electron curent, mA	1–15
Electron density, 10^{-8} cm^{-3}	1.6–23.5
Magnetic field, kG	1–3
Deviation of the magnetic field from parallel, $B_\perp/B$	5×10^{-5}
Length of cooling segment, m	2.4

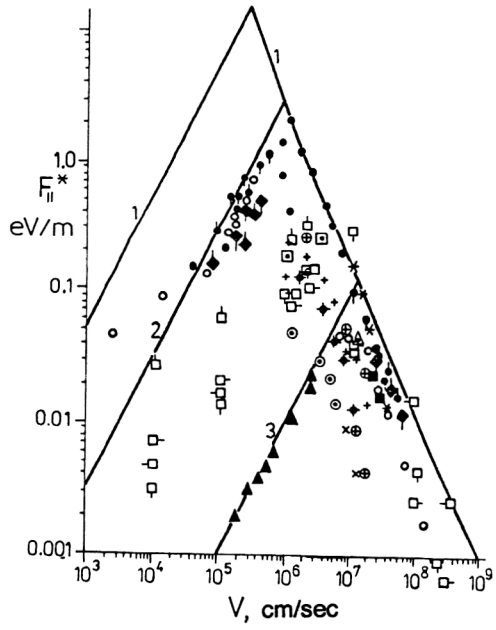

FIG. 14. Results of measuring the longitudinal friction force (Refs. 23, and 35–38): $F^*=F_\parallel/z^2 n_e^*$, where $n_e^*=10^{-8}$ cm$^3\cdot\eta n_e\gamma^{-1}$ is the "reduced" electron density in the particle frame. The solid lines are the calculation using Eqs. (1.36) and (1.37) for $n_e=10^{-8}$ cm^{-3} and various values of $\Delta_\parallel$ (cm/sec): 3.4×10^5 (*1*); 1×10^6 (*2*); 1×10^7 (3).

Symbol	Setup	Particles	Energy (MeV/nucleon)
✦	NAP-M	protons	65
●	MOSOL	protons	0.85
▲	ICE	protons	47
○	IUCF	protons	45
⊕	LEAR	protons	49
+	TARN	protons	20
⊡	CELSIUS	protons	180
⊙	CELSIUS	deuterons	783
△	CELSIUS	O^{8+}	296
✦	TSR	deuterons	12
●	TSR	Li^{3+}	12
◆	TSR	C^{6+}	12
◆	TSR	O^{8+}	12
■	TSR	S^{16+}	12
*	CRYRING	deuterons	12.2
□	ESR	C^{6+}	250
□	ESR	Ti^{22+}	250
□	ESR	Xe^{54+}	250
□	ESR	U^{92+}	250

23, Fig. 12) or the particle energy (ESR, Ref. 38). A selection of points on these curves is shown in Fig. 14.]

The question of the fine details of the physics of cooling in this region essentially remains open. Some of the specific features of the interaction at superlow velocities are discussed in Sec. 5.

4. THE COOLING ELECTRON BEAM

4.1. Electrostatic acceleration and the flattened distribution

In an electron beam of low intensity a flattened distribution of the type (1.26) has a kinetic origin.[8] This is most easily demonstrated in the nonrelativistic case: an electron emitted by a thermionic cathode at temperature T_c and accelerated in an electrostatic field by a potential difference U_0 has kinetic energy

$$\mathscr{E}=\mathscr{E}_c+eU_0=\frac{m}{2}(v_0+\Delta v)^2;$$

$$\frac{mv_0^2}{2}\equiv eU\equiv\mathscr{E}_0,$$

where $\mathscr{E}_c$ is the kinetic energy of the electron at the cathode. From this we find the velocity spread and the temperature of the longitudinal degree of freedom of the electrons in the frame moving with velocity v_0:

$$\Delta_\parallel\approx\frac{T_c}{mv_0},\quad T_\parallel\equiv m\Delta_\parallel^2\approx\frac{T_c^2}{2\mathscr{E}_c}.$$

It is possible to find $T_\parallel$ more rigorously[25] by writing the distribution in the electron energy $\mathscr{E}_c$ at the cathode as

$$f(\mathscr{E}_c)=A\cdot e^{-\mathscr{E}_c/T_c},\quad A=\text{const}. \tag{4.1}$$

From energy conservation and the Lorentz transformations we find

$$\mathscr{E}_c=\sqrt{p^2c^2+m^2c^4}-(\mathscr{E}_0+mc^2)\approx\beta c(p-p_0)=\gamma mv_\parallel,$$

$$p_0\equiv\langle p\rangle=\beta\gamma mc, \tag{4.2}$$

where p is the longitudinal component of the electron momentum in the lab frame after the acceleration and $v_\parallel$ is the electron velocity in the frame moving with velocity $v_0=\beta c$.

Since the distribution function is the integral of the collisionless Vlasov equation, if the total energy is chosen as the argument, $f(p)$ in (4.1) retains its form even after the acceleration. Substituting $\mathscr{E}_c$ from (4.2) into (4.1) and transforming the distribution function from the lab frame to the moving frame, after normalization to unity we find

$$f(v_\parallel)=\frac{\beta\gamma mc}{T_c}e^{-\beta\gamma mcv_\parallel/T_c},\quad v_\parallel>0. \tag{4.3}$$

The condition $v_\parallel>0$ reflects an obvious physical fact: only electrons moving "forward" enter the beam from the cathode. Therefore, $\langle v_\parallel\rangle\neq 0$, and the "longitudinal" temperature is

$$T_\parallel=m(\langle v_\parallel^2\rangle-(\langle v_\parallel\rangle)^2)=\frac{T_c^2}{\beta^2\gamma^2mc^2},$$

$$T_\parallel=\frac{T_c^2}{2\mathscr{E}_0}\approx 3\cdot 10^{-7}\ \text{eV}\quad\text{for}\ \mathscr{E}_0\ll mc^2. \tag{4.4}$$

The distribution (4.3) is not the equilibrium one. The beam relaxes to the state of thermodynamical equilibrium in a rather short time (see Sec. 4.3).

The electron transverse momentum is not changed in the acceleration, so that the transverse temperature is

$$T_\perp=T_c+T_{ab}(r),$$

where T_{ab} is the contribution of optical aberrations of the electron gun, which, in general, depends on the radial coordinate of the electron.

4.2. Fluctuations of the electron density and the longitudinal temperature

The electron density in beams used for cooling is high enough that the Coulomb interaction between the electrons can be neglected. Since the distances between electrons l_e fluctuate, the local electric field in the elecron gas is nonzero, and an electron in the gas possesses some potential energy, the so-called correlation energy, which for a hot gas is[39]

$$\mathscr{E}_{\text{cor}}=-e^3\sqrt{\frac{\pi n_e}{T}},\quad T\gg e^2n^{1/3}.$$

This situation occurs in the electron beam near the cathode, where the electron density is

$$n_c\sim n_e\sqrt{\mathscr{E}_0/T_c}\sim 1.5\cdot 10^{-3}\ \text{cm}^{-3}\ \ (T_c\sim 0.1\ \text{eV}),$$

so that $e^2n_e^{1/3}\sim 10^{-3}$ eV$\ll T_c$. For sufficiently rapid acceleration [see (4.6) below] the electron gas does not manage to "mix" and retains its initial structure. In this case the correlation energy of its electrons is of order of magnitude

$$\mathscr{E}_{\text{cor}}\sim-\frac{e^2}{\langle l_e\rangle}\sim-e^2n_e^{1/3}.$$

The oscillations executed by the electron under the action of the local electric field transform this potential energy into kinetic energy, which gives a contribution to the electron temperature $T_{\text{cor}}\sim-\mathscr{E}_{\text{cor}}$. This phenomenon can be demonstrated for the model of an "electron crystal" with a strictly cubic lattice and a single electron out of equilibrium (in its spacing). This system is equivalent to a "heavy hole–electron" dipole. Oscillating in the field of the hole with period $\tau=\pi\sqrt{2mr^3/e^2}$, the electron has time-averaged kinetic energy $\bar{\mathscr{E}}=e^2/r$. Taking the electron amplitude distribution to be Gaussian with dispersion l_e^2, we find $T=2\langle\bar{\mathscr{E}}\rangle=2\sqrt{2}e^2/(\pi l_e)\approx e^2n_e^{1/3}$. We also note that $\langle\tau\rangle\approx 2\pi/\omega_{pe}$.

As a result, the final electron temperature is

$$T_\parallel\sim\frac{T_c^2}{\beta^2\gamma^2mc^2}+e^2n_e^{1/3}\sim 3\cdot 10^{-7}-1\cdot 10^{-4}\ \text{eV}. \tag{4.5}$$

The time for the temperature to be established (thermalization of the beam) is determined by the plasma oscillations

[with frequency ω_{pe} (1.5)] and electron–electron collisions. In principle, this is the same Coulomb interaction process as electron cooling. In a magnetized beam this is case S in Eq. (1.36) for $F_\parallel$ with the condition $m=M$, which gives

$$\tau_{ee}=\lambda_s^{-1}\sim\frac{\Delta_\parallel^3}{2\pi n_e r_e^2 c^4 L_{MS}}\sim 10^{-9}\ \text{sec},$$

In an "ordinary" electron gun the acceleration is quite rapid:[40]

$$\tau_{\text{acc}}\simeq 3\,\frac{d}{v_0}\sim 10^{-9}\ \text{sec},$$

relaxation cannot occur during the acceleration time, and the electron temperature established right after the emission from the gun has a relatively high value:

$$(T_\parallel)_{\text{fast}}\sim e^2 n_e^{1/3}. \tag{4.6}$$

If the acceleration occurs fairly slowly, so that

$$\frac{1}{T_\parallel}\frac{dT_\parallel}{dt}<\min\{\tau_{ee}^{-1},\omega_{pe}\}, \tag{4.7}$$

the electron gas manages to relax during the acceleration, and the temperature at the exit from the gun is

$$(T_\parallel)_{\text{slow}}\sim\frac{T_c^2}{\beta^2\gamma^2 mc^2}. \tag{4.8}$$

The condition (4.7) at nonrelativistic energies can be written in terms of the average strength of the accelerating field E:

$$\frac{1}{T_\parallel}\frac{dT_\parallel}{dt}=\frac{1}{\mathscr{E}}\frac{d\mathscr{E}}{dt}=\frac{v}{\mathscr{E}}eE<\omega_{pe},$$

from which we find

$$E<\sqrt{\pi J\,\frac{m\beta c}{e}}\sim 3\ \text{kV/cm}. \tag{4.9}$$

The electric field in a Pierce gun is almost an order of magnitude higher, i.e., such a gun (operating according to the 3/2 rule) is fast, and the temperature of the electrons in its beam is given by Eq. (4.6). Attempts to make "slow" guns have been made recently (see Ref. 23).

4.3. Longitudinal–transverse relaxation

The flattened distribution in turn relaxes to a distribution which is isotropic, owing to electron–electron collisions: the cold longitudinal component is heated by the hot transverse components. In the absence of a magnetic field this process is none other than diffusion in an electron beam with a flattened distribution, and Eq. (1.40) for $m=M$ gives[41] ($\mathscr{E}_0\ll mc^2$)

$$\frac{dT_\parallel}{dz}\approx\frac{\pi e^3 J L_c}{\mathscr{E}_0}\sqrt{\frac{m}{T_\perp}}\approx 5\cdot 10^{-6}\ \text{eV/cm},$$

i.e., the longitudinal temperature increases by a factor of 10 over a distance of 2 m.

The diffusion process is significantly suppressed in a longitudinal magnetic field if

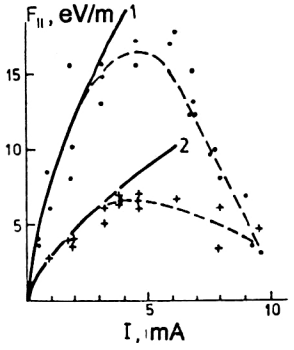

FIG. 15. Dependence of the maximum friction force on the electron beam current.[23] $B=3$ kG. Points: ●—negative H^- ions; ×—protons. Curves: $F=ke^2n_e^{2/3}$, for (1) $k_1=1.82$; (2) $k_2=0.72$.

$$\langle\rho_\perp\rangle\leqslant l_e=n_e^{-1/3}. \tag{4.10}$$

For the parameters of Table III this condition requires $B>1$ kG. For this magnetization (almost the maximum) the electron gas in the electron frame looks like a set of "Larmor circles" which slowly, with velocity $\Delta_\parallel$, travel along the field and collide with each other, exchanging momenta $m\Delta_\perp$. Therefore, the factor $\Delta_\parallel/\Delta_\perp$ appears in the diffusion power (1.40):

$$\left(\frac{dT_\parallel}{dz}\right)_{\text{magn}}\approx\frac{\pi e^3 J L_c}{\mathscr{E}_0}\sqrt{\frac{mT_\parallel}{T_\perp^2}}\approx 10^{-7}\ \text{eV/cm}. \tag{4.11}$$

5. THE FINE POINTS OF ELECTRON COOLING

5.1. The friction force for negatively charged particles

Negatively charged particles (antiprotons, negatively charged ions) repel electrons, while positively charged particles attract them. In collisions with parameters $\rho<\rho_{\min}$ in the first case a magnetized electron is reflected and transfers a momentum $2mV$ to the particle, while in the second case it passes near the particle without transferring any appreciable momentum to it. Therefore, for a negatively charged particle the longitudinal component of the friction force is increased by

$$\Delta F_\parallel=-n_e V 2mV\pi\rho_{\min}^2\sim-\frac{2\pi q}{m}\times\begin{cases}1/V^2, & V>\Delta_\parallel,\\ V^2/\Delta_\parallel^4, & V<\Delta_\parallel,\end{cases} \tag{5.1}$$

and the maximum value of the longitudinal component [see (1.36)] is

$$(F_\parallel^{(-)})_{\max}\sim-\frac{2\pi q}{m\Delta_\parallel^2}(1+L_{MS})\sim-2\pi e^2 n_e^{2/3}(1+L_{MS}). \tag{5.2}$$

This effect has been convincingly demonstrated in experiments at the MOSOL setup.[23,30] The experimental points in Fig. 15 in the region $I\leqslant 3$mA are approximated well by the function

$$F_\parallel=ke^2n_e^{2/3},\quad k=\begin{cases}1.82 & \text{for negatives ions}\\ 0.72 & \text{for protons.}\end{cases}$$

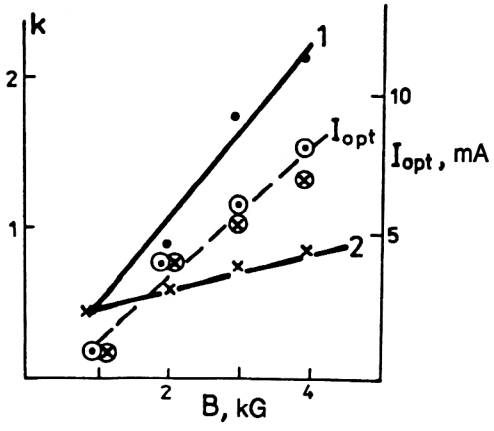

FIG. 16. Magnetic-field dependence of the coefficients k_1 and k_2 and the optimal value of the electron current.[23]

The falloff of the friction force in the region $I \leqslant 3$mA is due to the worsening quality of the electron beam as the current increases (increase of the longitudinal temperature along the beam owing to longitudinal–transverse relaxation, the influence of the space charge of the electron beam, and so on). This confirms the magnetic-field dependence, shown in Fig. 16, of the value of the beam current at which $F_\parallel$ reaches a maximum (dotted line); I_{opt} grows linearly with the field. There we also show the field dependence of the coefficient k. As the magnetic field increases, the difference between k_1 and k_2 grows significantly.

5.2. Diffusion of cooled protons

The particle beam and the cooling electrons meet on the cooling section at the exit from the toroidal section (Fig. 2). In the particle frame the beam extraction looks like a fast displacement of the electrons in the direction perpendicular to the axis of the beam of cooled particles:

$$\Delta z \approx \frac{(\beta c \Delta t)^2}{2R}, \tag{5.3}$$

where R is the radius of curvature of the electron trajectory in the toroidal solenoid. For the parameters of Table III this estimate gives a displacement of order 1 mm over a cyclotron revolution period (here $\rho_\perp \approx 0.02$ mm). i.e., the particle and the electron meet "instantaneously." If the particles are already cooled to the level $V \leqslant \Delta_\parallel$ and have positive charge, the electron and the particle move together, and the electron oscillates along the direction of the magnetic field under the action of the particle field, while simultaneously rotating slowly with frequency ω_d (drifting) around the field line passing through the particle. This is the well known drift in crossed fields: the longitudinal magnetic field and the transverse electric field of the particle. The force acting on the particle due to the electron changes direction with the electron drift frequency

$$\omega_d \sim c \frac{ze}{\rho^3 B}, \tag{5.4}$$

and the components, transverse to the field, of the momentum transferred by this force to the particle during the travel along the cooling section τ are

$$\Delta p_{x,z} \sim \int_0^\tau \frac{ze^2}{\rho^2} \times \begin{Bmatrix} \sin \omega_d t \\ \cos \omega_d t \end{Bmatrix} dt.$$

From this we have

$$\Delta p_\perp^2 = \Delta p_x^2 + \Delta p_z^2 = \left(\frac{ze^2}{\rho^2} \frac{2}{\omega_d} \sin \frac{\omega_d \tau}{2} \right)^2.$$

Averaging this quantity over a large time interval $\Delta t \gg \tau_0 > \tau$ (i.e., a large number of particle passages through the cooling section with period τ_0), we find the addition to the diffusion power:[23]

$$\begin{aligned} \delta Q &= \frac{1}{2M} \frac{1}{\tau_0 \sigma_{\max}} \int_0^{\rho_{\max}} \Delta p_\perp^2 2\pi \rho d\rho \\ &= \frac{4 \cdot 2^{2/3}}{3M\tau_0} \left(\frac{B n_e z^2 e^5 \tau^2}{c} \right)^{2/3} \int_{x_{\min}}^\infty \frac{\sin^2 x}{x^{7/3}} dx \\ &\approx 4\eta \frac{\tau^{1/3}}{M} \left(\frac{eBq}{c} \right)^{2/3}, \end{aligned} \tag{5.5}$$

where $x_{\min} = 4cze\tau n_e / B \ll 1$, $\eta = \tau/\tau_0 = l/C$, and $\rho_{\max} = l_e/2 \sim 1/2n_e^{1/3}$. Substitution of this addition (including η) into the Langevin equation gives, instead of (1.41),

$$\begin{aligned} T_p &\simeq T_\parallel (1+\delta), \\ \delta &\sim \frac{1.5}{L_{MS}} \left(\frac{\omega_B^2 \tau}{z^2 \omega_{pe}} \right)^{1/3} \approx 7 z^{-2/3}. \end{aligned} \tag{5.6}$$

This effect is quite clear when the particle is a proton and is accompanied by a single electron. It can become decisive for large B, because δ grows as $B^{2/3}$. The case of multiply charged ions is much more complicated.

5.3. The cooling of multiply charged ions

Let us begin with a rather obvious effect: the dependence of the Coulomb logarithms on the ion charge. It can significantly decrease the friction force (the decrement). In Fig. 17 we show the results of processing the experimental data obtained at the TSR for the cooling of multiply charged ions.[33] These experiments were carried out at ion energies of 5–12 MeV/nucleon, and the electron transverse velocity in them was $(6-8)\times 10^5$ cm/sec, i.e., the data given in Fig. 17 refer to superlow particle velocities (cf. Fig. 14).

For superlow particle velocities the binding effect described in the preceding subsection can also come into play. An electron oscillating around a positively charged particle vanishes at the exit of the cooling section just as suddenly as it appeared at the entrance to this section [see Eq. (5.3)]. Here it carries a longitudinal momentum whose sign depends on the phase of the oscillations at the instant when the exit is made. A rough estimate of this effect can be made by assuming that the oscillation frequency of the electron in the ion field (along the magnetic field) is

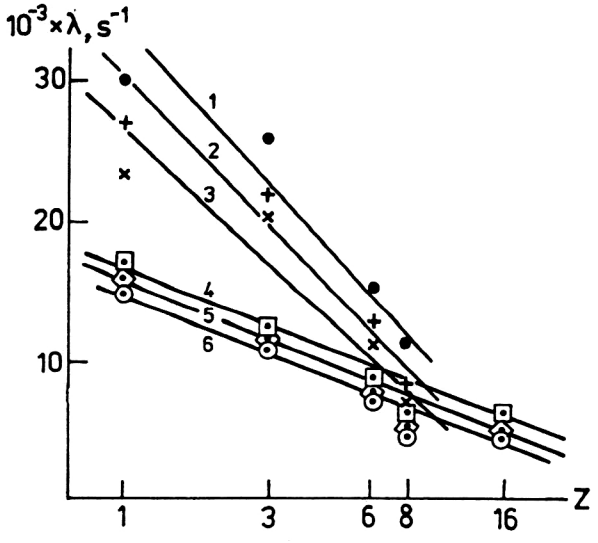

FIG. 17. Dependence of the longitudinal decrement on the ion charge z for various values of the transverse ion velocity (analysis of the results of Ref. 33): $\lambda^*=(A/z^2)\cdot(\lambda_\parallel/n_e^*)$, $n_e^*=10^{-8}n_e$.

Symbol	● + ×	□ ◇ ⊙
Curve	1 2 3	4 5 6
$V_\perp$, 10^5 cm/sec	6 7 8	6 7 8
n_e, 10^8 cm	0.72	3.42

$$\omega_\parallel\sim\sqrt{\frac{ze^2}{2m\rho^3}}, \tag{5.7}$$

where the impact parameter ρ is

$$\rho\leqslant\frac{l_e}{2}\sim\frac{1}{2n_e^{1/3}}. \tag{5.8}$$

Substitution of the upper limit gives the minimum frequency

$$\omega_\parallel\geqslant\sqrt{\frac{z}{\pi}}\,\omega_{pe}\sim10^9\sqrt{z}\ \text{sec}^{-1}. \tag{5.9}$$

This estimate shows that during the time of travel along the cooling section ($\tau\sim10^{-8}$ sec) the electron manages to complete several oscillations. Since $V<\Delta_\parallel$, the electron motion in the particle frame can be written approximately as

$$s(t)\approx s_0\cos\omega_\parallel t+(v-V_\parallel)\frac{\sin\omega_\parallel t}{\omega_\parallel},$$

where s is the coordinate along the magnetic field and $V_\parallel$ is the component of the particle velocity in the electron frame parallel to the field. The momentum transferred to the particle by the electron at the exit is $m\dot{s}(\tau)$. Averaging over the interval Δt as in (5.5), we find

$$\Delta F_\parallel=-\frac{mV_\parallel}{\tau_0\sigma_{\max}}\int_0^{\rho_{\max}}\sin\omega_\parallel\tau\cdot2\pi\rho d\rho$$

$$=-3.35\,\eta mV_\parallel\omega_{pe}^{4/3}\tau^{1/3}\left(\frac{z}{4\pi}\right)^{2/3}\cdot\text{Int},$$

$$\text{Int}=\int_\alpha^\infty\frac{\sin x}{x^{7/3}}dx,\quad\alpha=\sqrt{\frac{z}{\pi}}\,\omega_{pe}\tau\sim6\sqrt{z}. \tag{5.10}$$

The relative contribution to the longitudinal friction force is [see Eq. (1.36)]

$$\delta=\frac{\Delta F_\parallel}{(F_\parallel)_{MS}}=\frac{2\Delta_\parallel^3\tau^{1/3}}{z^{4/3}c^2r_e\omega_{pe}^{2/3}L_{MS}}\,\text{Int}\approx\frac{1.85}{z^{4/3}}\,\text{Int}. \tag{5.11}$$

Therefore, the effect can be significant, and its sign depends on the value of α:

$$\text{for}\ \alpha>1,\quad\text{Int}\approx\frac{\cos\alpha}{\alpha^{7/3}};$$

$$\text{then}\ \delta\approx\frac{\cos\alpha}{\sqrt{2}\pi^{3/2}c^2r_en_e\tau^2L_{MS}}.$$

This case of a single bound electron does not fully describe the bremsstrahlung of a multiply charged ion in a cooling electron beam, when it is necessary to take into account the multiparticle interaction in which at least z electrons take part. This process is studied by numerical modeling, although it must be said that only preliminary results have been obtained.[42] A rough estimate of the effect can be made, taking into account the fact that all the electrons oscillate in phase with frequency ω_{pe} [indicated by its presence in (5.9)–(5.11)]. Then as in (5.10) we find

$$\langle(\Delta F_\parallel)_z\rangle\sim-\frac{mV_\parallel}{\tau_0}z\sin\omega_{pe}\tau,$$

$$(\delta_F)_z\sim-\frac{2\Delta_\parallel^3\sin\omega_{pe}\tau}{r_ec^2z\tau\omega_{pe}^2L_{MS}}\sim-\frac{0.1}{zz}\sin\omega_{pe}\tau. \tag{5.12}$$

Similarly, we can try to include the additional diffusion of a multiply charged ion at superlow velocities: the electron cloud rotates as a whole about the magnetic field line intersecting the ion with frequency

$$\omega_{dz}\sim\frac{cze}{R_0^3B}=\frac{\omega_{pe}^2}{4\pi\omega_B},$$

$$R_0\sim z^{1/3}l_e. \tag{5.13}$$

The transverse component $\Delta p_\perp$ transferred to the ion during the passage is strictly equal to zero for a uniform distribution of the electrons about the ion. Since the density fluctuates, the average over many passages is $\overline{\Delta p_\perp^2}\neq0$. It is important that the angular velocity of the cloud rotation does not depend in a first approximation on the location of an individual electron. We can therefore write

$$\overline{\Delta p_\perp^2}=\sum_{i=1}^{z}(\Delta\vec{p}_\perp)_i^2,$$

$$(\Delta\vec{p}_\perp)_i=\frac{ze^2}{R_0^3}\int_0^\tau\vec{R}(t)dt,$$

$$\vec{R}(t)=R(\vec{l}_x\sin\omega_{dz}t+\vec{l}_y\cos\omega_{dz}t).$$

From this we find

$$\overline{\Delta p_\perp^2}=\frac{1}{\tau_0}\left(\frac{ze^2}{R_0^3}\right)^2\left(\frac{2}{\omega_{dz}}\sin\frac{\omega_{dz}\tau}{2}\right)^2 n_e\int_0^{R_0}R^2 4\pi R^2 dR$$

$$=\frac{16\pi z^{5/3}}{5}\left(\frac{eB}{cn_e^{1/3}}\right)^2\sin^2\frac{\omega_{dz}\tau}{2};$$

$$\delta Q=\frac{\overline{\Delta p_\perp^2}}{2M\tau_0}. \tag{5.14}$$

As in (5.6), we find

$$T_p=T_\parallel(1+\delta_z), \tag{5.15}$$

$$\delta_z\sim 24z^{5/3}\frac{\omega_B^2}{\omega_{pe}^3\tau L_{MS}}\sin^2\frac{\omega_{dz}\tau}{2}, \tag{5.16}$$

and for $\omega_{pe}\tau\ll 1$, $\delta_z\approx 0.04z^{5/3}\dfrac{\omega_{pe}\tau}{L_{MS}}\approx 0.2z^{5/3}$.

This estimate, which is valid at large z, can therefore determine the temperature of multiply charged ions (see Sec. 6.1).

6. THE PHYSICS OF COLD BEAMS

6.1. The transverse dimension of the cooled beam

The final velocity spread and, accordingly, the transverse size of a *beam of low intensity* is determined by the parameters of the electron beam (1.41), (5.6), and (5.16). In experiments (Table V) dimensions of the cooled beam significantly greater than the theoretical limit have been observed. The difference is especially great for heavy ions. This discrepancy is apparently related to the insufficiently high quality of the magnetic field along the cooling section: the criterion $\alpha<\Delta_\parallel$ (Sec. 2.3) is not satisfied. In fact, the results given in Table V for beams of low intensity show that to reach the theoretical limit in these experiments it was necessary for the magnetic field to be uniform at a level $B_\perp/B\leqslant 1\times 10^{-5}$, which certainly was not the case.

As the beam intensity increases, two effects come into play and tend to increase the spread of the particle velocities: *the defocusing action of the space charge and intrabeam scattering.*

The space charge of the cooled beam creates electric and magnetic fields acting on the particles like a defocusing lens. This effect is well known in accelerators, where it produces a shift of the frequency of betatron oscillations,[43] which for a cylindrical beam is

$$\Delta\upsilon\equiv\frac{\Delta\omega_{\text{bet}}}{\omega_s}=\frac{r_p N}{2\pi\varepsilon\beta^2\gamma^3}\frac{z^2}{A}\frac{C}{l}, \tag{6.1}$$

where $\pi\varepsilon$ is the emittance of the cooled beam, r_p is the classical proton radius, ze and A are the charge and atomic weight of the particle, C is the perimeter of the storage ring, and l is the bunch length ($l=C$ in the absence of a high frequency). In approaching the nearest machine resonance a buildup of the betatron oscillations occurs with disappearance of particles on the walls of the accelerator chamber.

Electron cooling significantly damps the effect of resonances. A sort of self-regulation occurs: the beam is squeezed to a size where the frequency of the betatron oscillations approaches the resonance value. Beyond this it becomes stable and there is no particle loss. Therefore, for given beam parameters (N, z, and A) and storage-ring parameters ($\Delta\upsilon_s$), Eq. (6.1) describes the equilibrium value of the emittance of the cooled beam. This effect was discovered in experiments at the NAP-M (Ref. 23) carried out at a proton energy of 1.5 MeV (Fig. 18), where the experimental value $\Delta\upsilon\simeq 0.1$ was obtained.

In the ESR experiments[44] for $^{197}Au^{79+}$ and $^{129}Xe^{54+}$ ions it was found that the size of the cooled beam (the emittance) grows as $\sqrt{N}$ ($\Delta\upsilon=\text{const}$). The maximum value of $\Delta\upsilon$ was 0.02 in the experiments for a beam containing about 10^8 $^{129}Xe^{54+}$ ions. A similar result was obtained for C^{6+} ions at the TSR (Ref. 45): the emittance increased as $N^{0.43}$, which corresponds to a nearly constant value of $\Delta\upsilon$, equal, for example, for the parameters of this experiment, to 0.04. We note that the experiment was carried out near the bound resonance, and $\upsilon_H-\upsilon_V\approx 0.07$.

Therefore, the estimate of the admissible beam intensity (6.1) is completely applicable as a practical approximation.

6.2. The momentum spread, noise, and "crystallization"

The momentum spread of the particles in a cooled beam is to a large degree determined by intrabeam scattering.[46] This is basically the same thing as longitudinal–transverse relaxation (Sec. 4.3). Equation (1.28) for Q, transformed to the lab frame, can be written as

$$\frac{d}{dt}\left(\frac{\Delta p_\parallel}{p}\right)^2_{\text{IBS}}=\frac{8r_p^2 cL_c}{\beta^3\gamma^3\varepsilon^{3/2}\sqrt{\beta_\varepsilon}}\frac{N}{C}\frac{z^4}{A^2}. \tag{6.2}$$

Here L_C is the Coulomb logarithm, β_ε is the value of the betatron function of the storage ring, averaged over the orbit (it is assumed that $\beta_x\approx\beta_z$), C is the perimeter of the storage ring, and $\pi\varepsilon$ is the beam emittance. If the diffusion in intrabeam scattering exceeds the diffusion in the electron beam, the former determines the equilibrium momentum spread, which at superlow velocities is [see Eq. (1.36)]

$$\overline{\left(\frac{\Delta p_\parallel}{p}\right)^2}=\frac{2L_C}{\pi\beta^3\gamma^3 n_e L_{MS}}\left(\frac{\Delta_\parallel}{c}\right)^3\frac{1}{\varepsilon^{3/2}\sqrt{\beta_\varepsilon}}\frac{N}{C}\frac{z^2}{A}\frac{m}{m_p}, \tag{6.3}$$

where m_p is the proton mass. From this it follows that the equilibrium momentum spread in an intense cooled beam must grow as $z\sqrt{N/A}\,\varepsilon^{3/4}$. The experimental results indicate that the physics of deep cooling of a beam is more complicated. For example, in the early experiments at NAP-M (Refs. 13 and 31) it was discovered that there is a suppression of the momentum spread to the level $\Delta p/p=1.2\times 10^{-6}$ if the beam intensity does not exceed $N\sim 3\times 10^7$ particles (Fig. 19). For $N>3\times 10^7$ the spread increased sharply. We note that the minimum spread attained corresponds to a temperature of 10^{-4} eV in the particle frame, which for the parameters of the NAP-M experiment is in good agreement with the condition (1.41).

In experiments involving heavy multiply charged ions at the ESR (Refs. 38, 44, and 47) and at the TSR (Ref. 45) a different picture was observed (Fig. 19): for a wide range of ions in the energy range 150–290 MeV/nucleon the momen-

TABLE V. Parameters of cooled low-intensity beams.

Parameters	NAP-M (Ref. 23)		ESR (Ref. 38)	
Type of Particle	protons		$^{197}Au^{79+}$	$^{129}Xe^{54+}$
Energy, MeV/nucleon	1.5	65	290	250
Beam diameter, mm	1	0.2	0.4	0.4
Angular spread of beam, 10^{-5} rad	7.0	1.4	3.6	3.6
n_e, 10^8 cm^{-3}	0.05	2.4	0.1	0.05
$\Delta_\parallel/\beta c$, 10^{-5} rad	20	4	1.2	1.1
Factor δ (5.6), δ_z (5.16)	25	12	50	30
$T_{\text{theor}}=e^2n_e^{1/3}(1+\delta)$, 10^{-3} eV	0.63	1.14	1.6	0.75
T_{exp}, eV	0.015	0.026	150	80

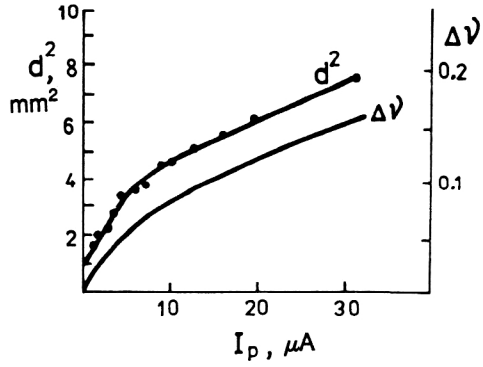

FIG. 18. Current dependence of the squared diameter of the proton beam and the calculated value of $\Delta\upsilon(d^2,I)$; $\mathscr{E}_p=1.5$ MeV, $I=1$ mA, $B=500$ G.

tum spread increases monotonically from the level 10^{-6}. (To be able to compare the experimental results, in Fig. 19 we have used the reduced linear particle density; see Sec. 6.7 below.)

Before discussing these results, let us return to Ref. 13. There the level of noise of a cooled proton beam was measured and used to find the particle momentum spread. The relation between these parameters was obtained in Ref. 14, where the physics of the noise of a particle beam in the presence of friction (cooling) was analyzed. In particular, the formation of space-charge waves in a beam circulating in a storage ring was studied for the first time. The main difference from linear beams is the existence of a particular relation between the particle momentum and the frequency of revolution in the storage ring, ω_s (Ref. 43):

$$\frac{1}{\omega_s}\frac{d\omega_s}{dt}=\eta_\omega\frac{1}{p}\frac{dp}{dt},\quad \eta_\omega=\frac{1}{\gamma^2}-\frac{1}{\gamma_{\text{tr}}^2}, \tag{6.4}$$

where $(\gamma_{\text{tr}}-1)Mc^2$ is the so-called critical energy of the storage ring. Taking into account this expression and using the approximation of long-wavelength perturbations and a narrow beam (the latter is well satisfied for a cooled beam), standard linear analysis (see, for example, Ref. 40) gives the phase velocity of the wave:

$$\upsilon_{\text{ph}}=\upsilon_0\pm\omega_pR_s,\quad \omega_p=\frac{z}{\sqrt{A}}\cdot\sqrt{\frac{\eta_\omega r_pc^2N}{\pi\gamma R_s^3}\ln\frac{b}{a}}, \tag{6.5}$$

where $R_s=C/2\pi$ is the average radius of the orbit and $a\ll b$ are the radii of the beam and chamber cross sections. The sign $\pm$ indicates that in the particle frame there are two waves traveling parallel and antiparallel to the velocity υ_0 with which they drift as a whole in the lab frame. Therefore, in the noise spectrum of the beam under certain conditions there appear two peaks separated by an amount

$$\Delta\omega_n=n2\omega_p,\quad n=1,2,\ldots . \tag{6.6}$$

This splitting (Fig. 20) exists if the following condition is satisfied in the cooled beam:

$$\omega_p=\Delta\omega_{\min}=\eta_\omega\omega_s\frac{\Delta p}{p}.$$

The stable state of the beam with split spectrum can, as a rule, be supported when there is sufficiently strong feedback which suppresses the growth of coherent oscillations of the particles: a so-called damper.[49]

As a rule, the experimental values of $\Delta\omega_n$ are in good agreement with the calculated values (6.6). Taking into account (6.5), this condition can be written as

$$N>N_{\text{th}}=\frac{A}{z^2}\frac{\pi R_s\eta_\omega\beta^2\gamma}{r_p\ln(b/a)}\left(\frac{\Delta p}{p}\right)^2. \tag{6.7}$$

Excess over the threshold value is a necessary condition for splitting of the peaks. The sufficient condition is more complicated to formulate. There are essentially two: the beam must be "deeply" cooled, and the intensity must satisfy (6.7). What does deeply cooled mean?

Here the idea of the ordering of the particle locations in the cooled beam arises. This was first pointed out in Ref. 24. The noise suppression for $N<3\times10^7$ in the NAP-M proton beam indicates the appearance of a significant correlation between the particle locations in the beam. The condition for such ordering to arise is known from solid-state physics (the so-called Wigner crystal; see Ref. 50 for details):

$$\frac{z^2e^2}{l_pT}\gg1,\quad l_p=n_p^{-1/3}, \tag{6.8}$$

where T and n_p are the temperature and density of particles with charge ze, and l_p is the average distance between particles. In this case the potential energy of the interparticle interaction exceeds the kinetic energy of the thermal motion. In the particle beam in a storage ring there are two parameters characterizing the distance between particles: the transverse dimension of the beam, a, and the longitudinal "gap" between the particles in the beam, $l_\parallel=C/N$. The condition (6.8) is obviously satisfied if

$$a<l_\parallel\ll\frac{z^2e^2}{T}. \tag{6.9}$$

It is interesting that the inequality (6.7) directly implies that the potential energy of a particle in a ordered beam chain is larger than the kinetic energy of the thermal motion:

$$\Gamma_\parallel\equiv\frac{z^2e^2}{l_\parallel}\Big/\frac{(\Delta p)^2}{2M_{\text{eff}}}>1. \tag{6.10}$$

Here

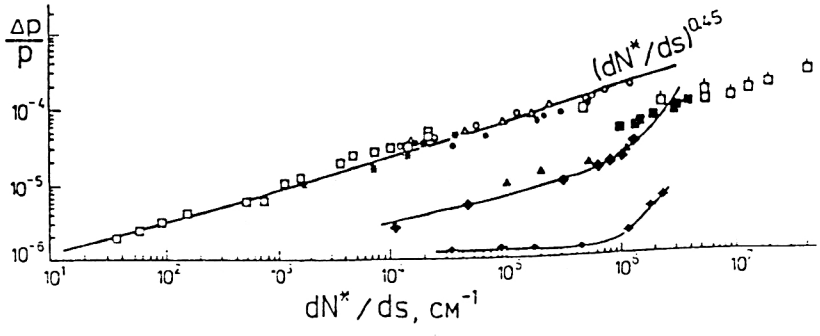

FIG. 19. Dependence of the particle momentum spread on the reduced linear density of the cooled beam:[23,41]

$dN^*/ds=(z^2/A)(N/\eta_\omega\beta^2\gamma^2 l)$, where l is bunched beam, C is free beam.

Symbol	●	□	*	⊙	△	●	♦	▲	■	□
Storage ring	NAP-M	ESR (upper curve)					ESR (lower curve)			TSR
Ion	p	$^{84}Kr^{36+}$	$^{129}Xe^{54+}$	$^{197}Au^{79+}$	$^{209}Bi^{82+}$	$^{238}U^{92+}$	$^{20}Ne^{10+}$	$^{40}Ar^{16+}$	$^{20}Ne^{10+}$	C^{6+}
Energy, MeV/nucleon	65	150	250	290	230	330	150	150	250*	5.3

$$M_{\text{eff}}=\frac{\gamma M}{\eta_\omega}\ln\frac{b}{a}$$

is some effective mass of the particle moving in a storage ring under the action of the wave field (the synchrotron mass multiplied by a logarithmic coefficient taking into account the mass of the wave field which carries the particles).

The two inequalities (6.9) also form the condition for "deep cooling." In experiments involving heavy ions, the results of which are shown in Fig. 19, this condition is not satisfied. As a result, the nature of the dependence of the momentum spread in the ESR and TSR ion beams and in the NAP-M proton beam differ fundamentally. It is interesting that in the NAP-M the noise suppression was observed up to $l_\parallel\sim 0.05$ mm for $a=0.1$ mm. In the ESR experiments the points Ne and Ar fall outside[45] the uniform dependence (the spread is roughly proportional to the square root of the linear particle density). For these points (with some optimism) it is possible to foresee a quasithreshold dependence of the spread on the reduced linear density, while the threshold value of the latter is the same (10^6 cm^{-1}) as for the NAP-M! Characteristically, the parameter $\Gamma_\parallel$ for the two curves below the threshold intensity was 3.7, while the parameter

$$\Gamma_\perp\equiv\frac{z^2e^2}{l_\parallel}\Big/T_\parallel$$

was significantly lower: 0.004 for the ESR and 0.012 for the NAP-M. For the upper curve (Au^{79+}, the point $dN^*/ds=10^4$), $\Gamma_\parallel\sim 6\times10^{-4}$ and $\Gamma_\perp\sim 1\times10^{-4}$.

Let us note another feature of the criterion (6.7). A parameter can, in general, take a negative value if the particle energy is above the critical value. In this case the threshold intensity is negative, and the plasma frequency (6.5) is imaginary. Physically, this implies that the particle revolution frequency falls with increasing momentum [see Eq. (6.4), $d\omega/dp<0$], and in their scattering the particles become grouped together: the so-called "negative-mass effect" in accelerators. All the experiments cited in the present study were carried out at an energy below the critical value ($\eta_\omega>0$). Of course, operation of the storage ring in the regime above the critical energy makes it impossible to obtain ordering of the particle locations in the beam. Another feature of the NAP-M was the fact that its operating regime was close to the critical energy ($\eta_\omega\approx 0.08$), as a result of which the threshold N_{th} (6.7) was lowered significantly.

The studies of Parkhomchuk *et al.* (Refs. 13, 14, and 24) initiated the physics of ultracold beams, where the main subject of interest is the realization in beams of the so-called crystalline state. Today there is no doubt about the possibility of ordering in the longitudinal direction, and the experiments of Ref. 13 have actually demonstrated this. As the beam intensity grows, the question of transverse ordering arises. Here an "existence theorem" has not yet been proved, although studies are being carried out very intensively (see the section entitled Crystallization in Ref. 4). The situation is rather the reverse: the impossibility of forming a two- or three-dimensional crystalline beam in a ring with soft focusing has been demonstrated.[51] The reason is again the negative-mass effect: it is well known that in a storage ring with soft focusing, $\eta_\omega<0$ for any energy. Nevertheless, a qualitative picture of the formation of such a beam has been around for some time (see, for example, Ref. 52): as the cooling becomes deeper, intense beams reach states in which an equilibrium crystalline structure is formed. First this structure is one-dimensional, then at higher intensity it is two-dimensional of the zig-zag type, and beyond it is three-dimensional (a spiral, coaxial cylindrical shells, and so on).

The problem of shear in passing through bending magnets remains unsolved: to preserve the crystalline structure, particles located at different radii must move with the same angular and, accordingly, different linear velocities, while on a straight section their velocities must be the same. This is possible only when there are significant oscillations of the

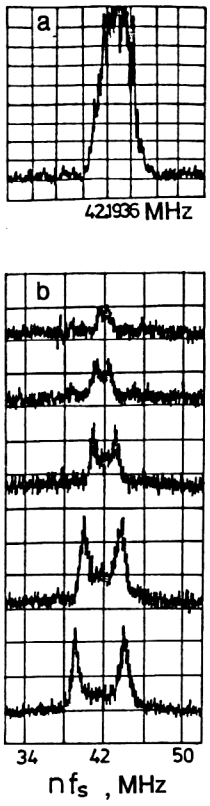

FIG. 20. Frequency spectrum of the Schottky signal of the cooled beam. (a) The LEAR storage ring (preliminary electron cooling of the antiprotons); 2×10^9 particles, the 40th harmonic of the revolution frequency, $\Delta p/p \cong \pm 1\times10^{-4}$, peak splitting not yet observed: $\omega_p \approx 500\ \text{sec}^{-1} \approx \Delta\omega$. (b) The TARN-II storage ring (Ref. 48): proton energy 16 MeV, measurements at the 60th harmonic of the revolution frequency, beam intensity equal to (from top to bottom)—2.6×10^7, 6.2×10^7; 1.4×10^8, 4.8×10^8, 8×10^8.

particles of the "crystal" about their equilibrium locations. And then the problem of stability, resonances, and so on arises.

What makes this state interesting? This is an ideal "natural model" of a condensed medium with a density 13–15 orders of magnitude below that of a solid object. The study of the "gaseous," "solid," and mixed states of such a medium and phase transitions, wave propagation, and heat-exchange processes in it should be very interesting.

The comparison of the experimental results from the NAP-M and from the ESR and TSR made here rather convincingly demonstrates the need for deep cooling in order to reach the crystalline state. A new level will be reached with the development of the laser cooling method (see Sec. 7.4).

7. COOLERS IN EXPERIMENTAL PHYSICS

7.1. A storage ring for intense cold beams

The choice of injection scheme usually determines the injector parameters. In a storage ring with electron cooling there exists a version of one-turn injection with storage of the particles on the separatrix of the phase motion. In this scheme a particle bunch is injected into an equilibrium orbit with the electron beam, the accelerating voltage of a high-frequency resonator, and a constant magnetic field switched on. As a result of the cooling in the beam, the momentum spread decreases and the particles are trapped on the separatrix and gathered into a short bunch. Then the next set of particles is injected, and the cycle is repeated many times. This scheme is attractive because it does not require large acceptance of the storage ring: the storage occurs in a "longitudinal phase space." Here the storage rate is limited by the time for the cooling of the longitudinal component of the momentum (2.10). The intensity of the stored beam is limited by its space charge (6.1).

There are plans to use the same injection scheme, which was proposed some time ago at the NPI in Novosibirsk, in the K4–K10 ion storage rings.[53,54] It turns out that it is more productive than the traditional versions of multiturn injection with storage in the transverse phase space. In the latter case the cooling action is slowed down considerably, owing to the large emittance of the beam injected in multiturn fashion.

In some cases multiturn injection with electron cooling can, nevertheless, ensure a good storage rate, especially when the particle energy is low. In particular, there is a proposal[55] to use this version for the storage of Pb^{53+} ions at LEAR with subsequent injection and acceleration in a cascade of accelerators at CERN for obtaining colliding proton–ion and ion–ion beams at the Large Hadron Collider (LHC).

7.2. A cooler with an internal target

Experiments at accelerators with electron cooling and an internal target have been under discussion in many contexts (Refs. 3, 9, 31, 53, and 54) since this was first proposed.[15] Among the principal advantages of such a setup are the high degree of monochromaticity of the beam and the precision with which the parameters of the reaction products are measured at high luminosity. The latter is described by the familiar relation

$$L = fNn_t l_t,$$

where f is the particle revolution frequency in the storage ring, N is the number of particles in an orbit, and n_t and l_t are the density and geometrical thickness of the target. For the typical parameter values $f=1$ MHz, $N=10^9$, and $n_t l_t = 10^{14}\ \text{cm}^{-2}$ the luminosity is $10^{29}\ \text{cm}^{-2}\ \text{sec}^{-1}$. In experiments with beams of "exotic" particles, in particular, radioactive nuclei,[53,54] the intensity can be limited to 10^6 particles, and then a thicker target becomes necessary. There are two principal physical limitations to the target thickness:

- the lifetime of the primary beam;
- the uncertainty of the energy of the primary and secondary particles in the target ("straggling").

The lifetime of a particle interacting with the target in a storage ring is determined by the same processes (Sec. 2.5) as in the absence of a target, except that when the target is present they are concentrated at its location. The diffusion processes are exactly the same: multiple scattering and ionization losses suppress electron cooling, while events of single recombination on the atomic electrons of the target, scattering beyond the aperture of the storage ring, and large single energy losses lead to a loss of particles. The contribu-

tion of single energy losses is usually negligible. Single scattering is described by an expression analogous to (2.14):

$$(\tau_\theta)_t = \frac{\beta^3\gamma^2}{4\pi Z_t^2 r_p^2 c}\left(\frac{A}{z}\right)^2 \frac{\varepsilon C}{n_t l_t \beta_t} \sim 12 \text{ min}, \qquad (7.1)$$

where β_t is the value of the betatron function at the target. From this we see that it is necessary to decrease β_t. For fixed lifetime this makes it possible to increase the target thickness and, accordingly, the luminosity.

For fully stripped ions the losses due to the change of their charge occur only as a result of recombination, the cross section for which for a wide range of elements in the energy range 1–100 MeV/nucleon is approximated by the dependence[56]

$$\sigma_{\text{rec}} \sim \frac{10^{-23} Z_t^{6.5} z^4}{(\mathscr{E}/A)^{6.66}}.$$

For example, for $^{48}Ca^{20+}$ ions and a magnesium target (Table III) this gives

$$\tau_{\text{rec}} \approx (f \sigma_{\text{rec}} n_t l_t)^{-1} \sim 230 \text{ sec}.$$

Therefore, this process can quite strongly limit the ion lifetime and, accordingly, the experimental luminosity.

The effect on the beam quality of particle multiple scattering on the target has special features in coolers. On the average it is suppressed by cooling: the *superthin target regime* (Ref. 15), but there are particles in the beam which are scattered at angles of the order of the aperture angle. This creates a *halo* of particles around a cold beam, which oscillate with large amplitudes and slowly return to the beam under the influence of the cooling.[31] The fraction of such particles can be found from the balance between the number of scatterings at angle θ per unit time and the cooling rate for particles with this amplitude [see (2.10)]:

$$\left(\frac{dN}{dt}\right)_{\text{scat}} = L \cdot d\sigma(\theta) = \frac{dN(\theta)}{\tau_{\text{lab}}(\theta)}.$$

From this we find

$$\frac{\Delta N(\theta_{\max})}{N} = \frac{Z_t^2}{3\gamma^2 A L_C} \frac{m}{m_p} \frac{n_t l_t}{(n_e)_{\text{lab}} l_{\text{cool}}} \left(\frac{\beta_t}{\beta_{\text{cool}}}\right)^{3/2} \theta_{\max},$$

where $(n_e)_{\text{lab}}$ is the electron density in the lab frame, m_p is the proton mass, l_{cool} is the length of the cooling section, and β_t and β_{cool} are the values of the betatron functions at the target and on the cooling section. For the parameters of Table III and $\theta_{\max} = 3$ mrad the halo amounts to a fraction of order $10^{-5} Z_t^2/A$ of the total number of particles, which can be significant for light ions ($A \sim 1$) and a heavy target (for example, uranium). To decrease the halo and also the effect of single scattering, it is necessary to minimize β_t.

Ionization losses in the target introduce an uncertainty into the value of the particle energy, owing to the spread in the locations of the points at which the particle interacts with the nuclear target throughout its thickness. This uncertainty is

$$\left(\frac{\Delta\mathscr{E}}{\mathscr{E}}\right)_{\text{ion}} = \frac{8\pi r_p r_e L_z}{\beta^4} \frac{z^2}{A} Z_t n_t l_t \sim 10^{-10} \frac{z^2}{A} Z_t,$$

where $L_z \sim 15$ is the Coulomb logarithm of the ionization losses. This estimate shows that this effect can determine the accuracy of precision experiments ($\Delta\mathscr{E}/\mathscr{E} \sim 10^{-6}$) with heavy nuclei and fragments. We note that the ionization losses also create a halo in the energy distribution of particles in a cooler; there are large deviations in the energy (the distribution tail), and the intensity of the halo is low.[31] This effect should be taken into account when designing experiments involving heavy ions.

Experiments in coolers with internal targets have essentially just begun. The first experience in working with storage rings in the presence of various types of jet targets (Refs. 17, 57, and 58)—gas, vapor, cluster, drop, and filament—has been obtained. The last two types of target have significant advantages over vacuum conditions. It should be noted that the years of experience gained in working with superthin internal targets at electron storage rings may prove to be a great help in such experiments.

The technique of using coolers with internal targets becomes especially interesting in studies of radioactive nuclei,[59,60] where it makes it possible not only to store intense beams of such nuclei, but also to perform precise measurements of their properties.

7.3. A precision mass spectrometer. Isomer separation

Using the focusing system of a storage ring as a spectrometer and the high degree of monochromaticity of the cooled beam, it is possible to measure an ion mass with an accuracy unobtainable by other methods: up to $\Delta M/M \sim 10^{-6}$. It is simplest to do this by measuring the particle revolution frequency according to the Schottky signal (Fig. 20) and to use the frequency shift to determine, for example, the isomer mass difference. Here a special feature of coolers arises: electron cooling keeps the ion velocities the same and equal to the electron velocity, so that for two isomers the mass resolution is[3)]

$$\frac{\Delta M}{M} = -\gamma_{\text{tr}}^2 \frac{\Delta\omega}{\omega} + (\gamma_{\text{tr}}^2 - \gamma^2)\frac{\delta v}{v} + \gamma^2 \frac{\delta B}{B}, \quad \delta v = \frac{V_\parallel}{\gamma^2}.$$

Here δB is the level of pulsations of the magnetic field of the storage ring and δv is the spread of ion velocities in the cooled beam [cf. (6.4)]. Of course, the stability of the electron cooling must be quite high in such experiments. Here the trick of "suspending" the cooling section under a small regulating potential with feedback to the source of the cathode potential works well.

The suspension trick works even better when spatial separation of the isomer orbits is necessary. For this a transverse velocity gradient can be created in the electron beam and a sufficiently large value of the dispersion function of the storage ring ψ_{cool} ensured on the cooling section. The first is obtained, for example, by placing on this section along the electron beam plates which create a uniform transverse field.[62] Then at the entrance to this section the electrons on the edge fields acquire (lose) an additional energy, so that the velocity gradient is

$$\Psi_e^{-1} \equiv \frac{1}{\beta c}\frac{dv_e}{dr} = \frac{eE_\perp}{2\mathscr{E}_e}, \quad \mathscr{E}_e \ll mc^2. \tag{7.2}$$

To avoid perturbing the electron trajectories by the field $E_\perp$ it is sufficient to impose a transverse magnetic field $H_{\perp\perp} = E_\perp/\beta$ so as to have crossed fields.[4)] The orbit of a particle with mass $M + \Delta M$ on the cooling section will then be shifted by the amount

$$\Delta r_{\text{cool}} = \psi_{\text{cool}}\left(\frac{\Delta v_p}{\beta c} + \frac{\Delta M}{M}\right),$$

which, taking into account the equality $\Delta v_p(r) = \Delta v_e(r)$ and (7.2), gives

$$\Delta r_{\text{cool}} = \psi_{\text{cool}}\frac{\Delta M}{MM}\frac{1}{1-\psi_{\text{cool}}/\psi_e}. \tag{7.3}$$

For $\psi_{\text{cool}} = 5$ m and $(\psi_e - \psi_{\text{cool}})/\psi_e = 10^{-2}$ the shift (7.3) amounts to 5 mm for $\Delta M/M = 1\cdot 10^{-5}$. The effect can be enhanced if a large dispersion is created at the point where the isomers are detected (collected) (increase of Δr in the ratio $\psi_{\text{Det}}/\psi_{\text{cool}}$). A difficulty of this method is the need to keep the small difference $\psi_e - \psi_{\text{cool}}$ stable and fixed. When these two terms are equal, particles are lost (see Sec. 2.4 and Fig. 8).

Another scheme for isomer separation[63] involves switching on an accelerating high-frequency voltage, whose frequency Ω compatible with the momentum of particles subject to removal from the beam. This potential is slowly varied with time, which shifts the orbit of these particles. The high-frequency potential must be low enough so that the "needed" particles lie outside the separatrix:

$$\frac{\Delta M}{M} > \frac{1}{\beta}\sqrt{\frac{2zeV}{\pi h \eta_\omega \gamma M c^2}}, \tag{7.4}$$

where h is the number of the high-frequency harmonic. The tuning of the frequency Ω must be fast enough that the electron cooling cannot keep the particle velocity constant (equal to the electron velocity) and, accordingly, hinder the particle acceleration:

$$\frac{1}{\Omega}\frac{d\Omega}{dt} = \eta_\omega \frac{1}{p}\frac{dp}{dt} > \frac{\eta_\omega}{\tau_{MS}}, \tag{7.5}$$

where

$$\tau_{MS} \approx \frac{\beta\gamma^2}{2\pi c r_p L_{MS}}\frac{mc^3}{\eta e J}\frac{A}{z^2}\left(\frac{\Delta_\parallel}{c}\right)^3 \tag{7.6}$$

is the cooling time (in the lab frame) of the particles in the beam cooled to superlow velocities [see Eqs. (1.36), (1.37), and (2.10)]. For the parameters of Table III, $\Delta M/M \sim 10^{-5}$ and $\eta_\omega \sim 1$, the conditions (7.4)–(7.6) give $V < 15A/z$ mV, and the frequency tuning time is $\Delta t < \tau_{MS} \sim 30A/z^2$ μsec. The last condition means that already for $z \gtrsim 30$ the frequency tuning time must be smaller than the particle revolution period in a "typical" storage ring. Therefore, the condition (7.5) makes the method applicable only for light ions.

Yet another advantage of cooler technology should be noted: the possibility of precise absolute measurements. The reference value here is the potential at the cathode of the electron gun, which can be measured with high absolute accuracy ($\Delta U/U \sim 10^{-6}$). From this and from the equality of the particle and electron velocities it is possible to reach the absolute values of the measured parameters. An important factor is that in such experiments there is another parameter which is absolutely measurable also with high accuracy: the particle revolution frequency. Knowledge of two parameters, the velocity and the frequency, makes it possible to eliminate the uncertainty in the location of the orbit.

7.4. Atomic physics. Laser cooling. Nuclear spectroscopy

The cooling electron beam is an ideal target for studying electron–ion recombination (including its spectroscopy). The use of the device of a suspended interval described in the preceding section here also makes it possible to control the relative velocity of the particles and electrons with high resolution. This is how the first precision measurements of dielectric recombination were carried out, using Au^{75+} ions at the ESR (Ref. 64) and Se^{23+} ions at the TSR (Ref. 34). Experiments of this type, especially ones involving ions which are deeply ionized, up to the bare nuclei, are of great interest for atomic physics, astrophysics, and plasma physics.

Here it is appropriate to mention the phenomenon of stimulated recombination (see, for example, Ref. 27): a laser beam accompanying particles and electrons on the cooling segment undergoes a resonance (when the wavelength of the laser is chosen appropriately) interaction with the ion–electron system, which considerably increases the recombination rate. The first experiments on stimulated recombination were carried out at the ESR (Ref. 64), using Ar^{18+} ions.

Another process related to the interaction of laser radiation with ions in a storage ring is laser cooling.[65] The mechanism of this process is closely related to the Doppler effect: the cooled particle (ion) absorbs a photon from the laser beam, which is directed precisely parallel (or antiparallel) to the average velocity of the particle, $\vec{v}_0$, and then emits it isotropically in its rest frame; therefore, the time-averaged momentum transferred to the particle by the radiation also points along the vector $\vec{v}_0$. The absorption cross section has a resonance dependence on the wavelength of the radiation and, accordingly, on the particle velocity (the Doppler effect). The force acting on the particle (accelerating or decelerating, depending on the direction of the beam) has the same resonance dependence (Fig. 21). If in some way an opposing force F_0 independent of the particle velocity is created, the existence of an equilibrium value of the velocity v_0 can be ensured. This is how laser cooling works. The opposing force is created by using an induced voltage across the gap of the vacuum chamber of the storage ring. Versions using a colliding laser beam or an hf resonator have also been proposed. In the latter case the particle beam is unavoidably bunched.

It is clear from this discussion that laser cooling acts only on the longitudinal component of the particle velocity. The possibilities of "indirect" laser cooling of the transverse degrees of freedom[66] by coupling (including specially devised) of the longitudinal and transverse motion of the particle in the storage ring are being discussed.

The main characteristics of laser cooling are easiest to obtain by transforming to the frame of an ion moving with velocity $\vec{v}_0+\vec{V}$, where $\vec{v}_0$ is the average ion velocity in the beam. The friction force in this frame can be written as (Fig. 21a)

$$F(V_\parallel)=\frac{\hbar\omega'}{c}\,\sigma(V_\parallel)\,\frac{d\dot{N}}{ds}-F_0,$$

where $\omega'=\gamma(1-\beta)\omega_L$ is the frequency of the laser radiation in the ion frame, ω_L is the same in the lab frame, $\beta=(v_0+V_\parallel)/c$, $\gamma=(1-\beta^2)^{-1/2}$, $\hbar\omega'(d\dot{N}/ds)=dP_L/ds$ is the power of the laser radiation in the ion frame (for simplicity, this is small compared with the so-called saturation intensity; see, for example, Ref. 67),

$$\sigma(V_\parallel)\simeq\lambda_\omega^2\,\frac{(\Gamma/2)^2}{(\omega'-\omega_0)^2+(\Gamma/2)^2}$$

is the radiation absorption cross section,[68] ω_0 and λ_ω are the transition frequency and wavelength, and Γ is the line width. Then the decrement [free particle; see (2.2)] is

$$\lambda_L=-\eta\,\frac{2}{M}\,\frac{\partial F}{\partial V}\bigg|_{V_\parallel=V_{st}}=\eta 6\sqrt{3}\pi^2\,\frac{\gamma_0^2}{M\omega_0\Gamma}\,\frac{dP_L}{ds},$$

where $\gamma_0=(1-v_0^2/c^2)^{-1/2}$, and η is the ratio of the length of the cooling segment and the perimeter of the storage ring. The numerical estimates given in Table VI show that λ_L reaches huge values, but, unfortunately, only in a very narrow range of velocities:

$$\Delta V_\parallel\sim\frac{\Gamma}{\gamma_0^2\omega_0}\,c\sim(10^2-10^3\ \text{cm/sec})/\gamma_0^2.$$

Therefore, laser cooling operates fairly effectively only in an ion beam which has undergone preliminary electron cooling.[65]

The temperature established in a beam of laser-cooled ions is determined by the equilibrium of the power of the friction force $\bar{P}_{st}$ and the diffusion power $\bar{Q}_{\text{dif}}$ arising from fluctuations of the radiation (primarily, the isotropy of the ion radiation):

$$\bar{P}_{st}=-\eta\left(\frac{\partial F}{\partial V}\right)_{st}\overline{V^2},$$

$$\bar{Q}_{\text{dif}}=\frac{\eta}{2M}\cdot\langle(\Delta p)^2\rangle_\Omega\sigma(V_{st})\,\frac{d\dot{N}}{ds},$$

where $\langle(\Delta p)^2\rangle_\Omega=\frac{1}{3}(\hbar\omega_0/c)^2$ is the value of the squared momentum of the ion radiation, averaged over solid angle. Performing the corresponding substitutions and calculations, we find the established ion temperature:

$$T_\parallel=M\overline{V^2}\simeq\frac{\hbar\Gamma}{6\sqrt{3}}.$$

This limiting value of the temperature, which does not exceed several hundred μK (Table VI), can be attained in ion beams of low intensity, when the effect of intrabeam scattering is negligible (we note that inclusion of the saturation effect gives a value of $T_\parallel$ which is about twice as large[65]).

Another drawback of laser cooling in addition to its highly resonant behavior in the ion velocity is the small number of "candidates" for the use of this method. Practically all of them (which have been developed up to now!) are shown in Table VI. This paucity is due to the restricted choice of lasers with suitable wavelength. As laser technology develops, the possible candidates will increase in number.

The first successes in laser cooling were attained at the TSR and ASTRID accelerators (see the section on laser cooling in Ref. 4). Cooling of the longitudinal velocity component for all three candidates was obtained, and recently[34] at the TSR indirect cooling of the transverse component has been obtained (though with very small decrement $\sim 1\ \text{sec}^{-1}$).

Laser cooling is of exceptional interest from the viewpoint of obtaining ultracold ion beams. This may be very promising in particular for the problem of beam crystallization (Sec. 6.2). The recombination experiments described at the beginning of this section will reach a new level: in the past in atomic physics it was nearly impossible to work with such cold objects while controlling and varying their parameters with such accuracy.

Another application of the methods of electron and laser cooling might be the laser spectroscopy of nuclear states:[69] here the use of cold beams might make it possible to significantly increase the experimental sensitivity and accuracy.

7.5. High-energy physics

The use of electron cooling in high-energy physics has been discussed repeatedly (Refs. 1–3, 9, 19, and 31). Today the possible applications have reduced to three proposals:

(1) the storage and formation of a dense, intense beam of lead ions at the LEAR storage ring as part of the LHC project at CERN;[55]

(2) colliding proton–antiproton beams in the energy range 2–10 GeV as part of the SuperLEAR project at CERN;[70]

(3) high-voltage cooling in the relativistic heavy-ion collider RHIC at Brookhaven.[71]

The first proposal (see also Sec. 7.1) is apparently the closest to being realized. The second, which has the ultimate goal of precise measurements of the parameters of meson resonances (Ψ, Y) in deeply cooled $p\bar{p}$ beams, unfortunately has practically no chance of being realized, owing to economic reasons, in spite of the great interest in the project on the part of the scientific community. It is appropriate to note that now in Russia we have also lost our very good chance of having rich antiproton physics, as the proposals (see Ref. 72) have been rejected.

The third proposal looks rather realistic (although it also may not be realized) and represents a limiting case of the use of electronic cooling: the electron energy in the range 1–3 MeV is a reasonable technical limit of the method in the version with a single-pass (noncirculating) electron beam.

8. ANTIHYDROGEN AND THE CPT THEOREM

The idea of producing antihydrogen atoms arose[9] soon after the first experiments on electron cooling were per-

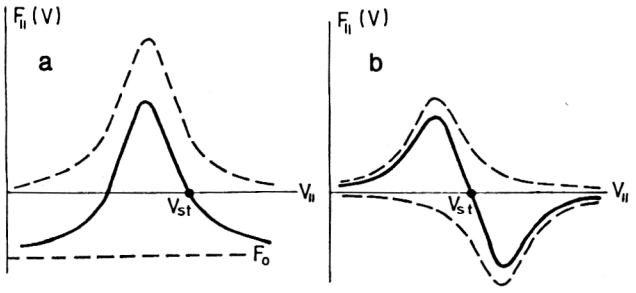

FIG. 21. Dependence of the "laser friction" force on the ion velocity in the particle frame. (a) Scheme with induced deceleration; (b) scheme with two lasers; the dotted line is the velocity dependence of each of the two forces acting on the ion, and the solid line is the resulting force; V_{st} is the equilibrium point.

formed and has been under discussion many times since then (see Ref. 73 and literature therein). Antihydrogen production is of interest not only for "philosophical" reasons—it is the simplest physical antimatter system—but also for practical reasons: it can be used to check the CPT theorem by comparing the hydrogen and antihydrogen emission spectra. It is expected that a difference in the hyperfine structure of the spectra may appear at the level $\Delta\omega/\omega \sim 10^{-18}$.[77] At present it is hoped that it will be possible to carry out such experiments by storing in magnetic traps antihydrogen atoms produced in antiproton interactions with a target. The probability for this process is extremely low, primarily owing to the smallness of the cross section for incidental positron production. Nevertheless, it is assumed that even several atoms captured in a trap are sufficient for the necessary measurements.

Budker and Skrinskiĭ[9] have proposed that an antiproton storage device be combined with a positron one in which the beam is cooled radiatively. This necessarily requires relativistic energies, so that significant technical difficulties will arise.

The problem is simplified if one works at low energy and uses electron cooling not only for the antiprotons, but also for the positrons. The first such proposal[18] was based on the use of a longitudinal magnetic field for focusing the positrons (energy of order 50 keV) on the cooling section. In this case at the entrance to the field the positrons acquire significant azimuthal velocities $v_\perp = \omega_B r/2$, where r is the distance

TABLE VI. Candidates for laser cooling (Ref. 65).

Parameters	$^{6,7}Li^+$	$^{9}Be^+$	$^{24}Mg^+$
Lower state	$2s^3S_1$ ($F=2, 5/2$)	$2s^2S_{1/2}$	$3s^2S_{1/2}$
and its lifetime, sec	50	ground state	ground state
Higher state	$2p^3P_2$ ($F=3, 7/2$)	$2p^2P_{3/2}$	$3p^2P_{3/2}$
and its lifetime, nsec	43	8.2	3.5
Line width, MHz	3.7	19.4	45.5
Wavelength of transition, nm	548	313	280
Saturation intensity, mW/cm^2	2.9	83	270
F_{max}, meV/m	8.8	81	210
λ_{max}, 10^4 sec^{-1}	5.7	14	6.4
$T_\parallel$, μK	62	330	770

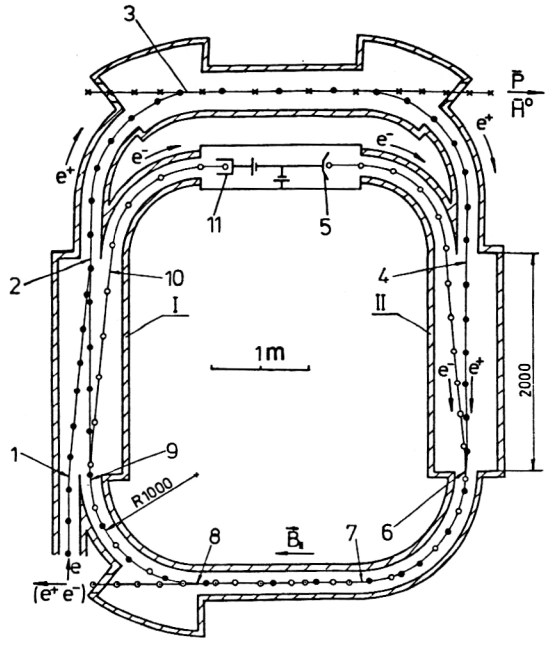

FIG. 22. Scheme for an antihydrogen generator: I and II are the input–output section and the section for withdrawal of the positron and electron beams (septums); *1–11* are the positions of the positrons and electrons (explanations in the text).

to the solenoid axis. This makes it necessary to decrease the transverse size of the beam, or else the efficiency of positron cooling falls. This limitation creates difficulties for the design as a whole, because the emittance and, accordingly, the intensity of the positron beam is lowered, which leads to a decrease of the antihydrogen yield.

Such difficulties can be eliminated by working with completely magnetized beams of electrons and positrons.[74] In this case the positron source (for example, a target bombarded by electrons or hard x rays) is located inside a solenoid at a positive potential suitable for accelerating low-energy positrons (a "positron gun"). The problem of controlling the motion of the electrons and positrons is solved as follows. The positron ring (Fig. 22) is made of two straight solenoids, four toroidal solenoids, and two special solenoid–septums. The latter, in addition to the basic windings producing the longitudinal field $\vec{B}_\parallel$, contain two other transverse-field windings, one inside the other (Fig. 23). Kicker coils forming a pulsed field parallel to the torus axes are located inside toroidal section 2–3. In addition, in all four toroidal sections there are windings of the constant transverse field, also oriented along the torus axis, which ensures motion of the positrons in a closed orbit after the kicker is switched off. Positrons and a combination of e^+e^- beams are injected by using the particle centrifugal drift arising on the toroidal sections if the transverse field is not matched to their momentum and the sign of the charge. For example, positrons injected above the median plane of the ring are displaced in the upper gap of the septum I and drift downward when the kicker in section 2–3 is switched on, leaving on an axial trajectory. After a single revolution the kicker is switched off. Electrons from the gun 5 move in

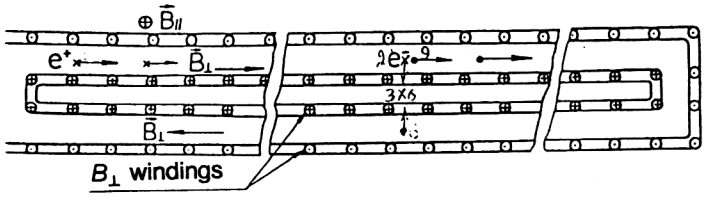

FIG. 23. Particle motion inside the septums.

static magnetic fields, enter the septum II below the median plane, are displaced to the point 6, drift upwards on section 6–7, interact with positrons on the cooling section 7–8, and again drift upwards (8–9) and to the right in septum I (9–10), reaching the collector 11. The entire positron ring is imbedded in the linear gap of the antiproton storage ring, just as is done for the electron cooling system (Fig. 22).

The physics of the electron cooling of positrons is the same as for heavy particles. The magnetization of the positrons is manifested in rather deep cooling, so that the cooling time can be estimated by using Eq. (2.10) with M replaced by m. The equilibrium state of the magnetized positrons requires special analysis. From very general considerations it can be shown that their transverse temperature at least does not exceed the transverse temperature of the electrons.

Although the cooling of positrons in a longitudinal magnetic field does not contract the beam, it significantly lowers the temperature, which raises the recombination rate. To increase the positron density, the target (gun) can be placed in a field smaller by a factor of 3–5 and adiabatic compression of the beam can be used.

We note that on the positron cooling section there is "incidental" production of a bound e^+e^- state—long-lived orthopositronium, which is of independent interest. Short-lived parapositronium has a decay length of about 1.5 cm at an energy of order 50 keV and does not deplete the positron beam.

In Table VII we give the main parameters of the antihydrogen generator. The intensity of the positron beam is limited by space-charge effects. The positron yield will be considerably higher if it is possible by electron cooling to lower the positron temperature to the level of $T_{\parallel}$.

A final question: what should be measured once we have an antihydrogen beam, and how should it be measured? "What" is clear: the hyperfine structure of the spectrum. "How" may be answered by the many-years-long experiments of Sokolov *et al.*,[75] who have used an original "atomic interferometer" to measure successfully the Lamb shift in hydrogen atoms on the $2P_{1/2}-1S_{1/2}$ transition with an accuracy of $\Delta\omega/\omega\sim 1\times 10^{-13}$, which today is a record. In these experiments the atoms had thermal velocities. Similar experiments, but involving fast atoms created in recombinations on the cooling section of the NAP-M, were performed in the 1970s by Parkhomchuk (with significantly lower accuracy).[76] Reaching the level 10^{-18} is, of course, a serious problem.

TABLE VII. Parameters of the antihydrogen generator.

Antiproton energy, MeV	55
Positron and electron energy, keV	30
Perimeter of positron ring, m	21.5
Length of cooling and recombination sections, m	1.5
Magnetic field strength, T	0.1
Intensity of antiproton beam	1×10^{11}
Intensity of positron beam	1×10^{10}
Density of electron beam, A/cm^2	1.0
Angular spread of positrons before cooling, mrad	50
Time for positron cooling, sec	0.4
Diameter of positron beam, mm	2
Flux of antihydrogen atoms, sec^{-1}	2×10^5
Orthopositronium flux, sec^{-1}	1.5×10^5

CONCLUSION

Experience in the development and use of the electron cooling method has shown that it can be used effectively in a fairly wide range of cooled particle energies, from a fraction to hundreds of MeV/nucleon. The rich experimental possibilities revealed when this method was developed are now only in the initial stage of their realization. Many important achievements can certainly be expected in this area.

The author would like to take this opportunity to sincerely thank J. Bosser, V. A. Lebedev, D. Mel, Yu. Ts. Oganesyan, V. V. Parkhomchuk, A. N. Skrinskiĭ, E. M. Syresin, and G. M. Ter-Akop'yan for many years of fruitful collaboration, and also A. V. Smirnov and O. G. Stepashkin for help in preparing the manuscript.

[1)]Actually, the lifetime according to this effect of a particle circulating in a storage ring is $\tau=(\sigma n_0)\sim(10^{-26}\ \text{cm}^2\cdot 10^{15}\ \text{cm}^{-3}\cdot 10^{10}\ \text{cm/sec})^{-1}=10$ sec, where σ is the nuclear interaction cross section, n_0 is the average absorber density along the trajectory, and v is the particle velocity.

[2)]We note the following relation, which is obvious but very convenient for numerical estimates: the values of the proton and electron energies have the same ratio as the masses when the velocities are equal (relativistic velocities), namely, 1836.1. In the case of ions this statement is valid for the energy per nucleon.

[3)]If δp and δM are free parameters, then[61]

$$\frac{\Delta M}{M}=\gamma_{\text{tr}}^2\left(-\frac{\Delta\omega_s}{\omega_s}+\eta_\omega\frac{\delta p}{p}+\frac{\delta B}{B}\right).$$

[4)]A similar device with crossed fields is known in ion optics as a Wien filter, where it serves to separate particles with different velocities.

[1] G. I. Budker, in *Proc. of the Intern. Symp. on Electron and Positron Storage Rings*, Saclay, 1966, p. II-I-I; At. Energ. **22**, 346 (1967).
[2] Report of the VAPP-NAP Group, in *Proc. of the Eighth Intern. Conf. on High Energy Accelerators*, CERN, Geneva, 1971, p. 72.
[3] A. N. Skrinskiĭ and V. V. Parkhomchuk, Fiz. Elem. Chastits At. Yadra **12**, 557 (1981) [Sov. J. Part. Nucl. **12**, 223 (1981)].
[4] *Proc. of the Workshop on Beam Cooling and Related Topics*, Montreaux, 1993, CERN, Geneva, 1994.
[5] G. I. Budker, N. S. Dikanskiĭ, V. I. Kudelaĭnen *et al.*, in *Proc. of the Fourth All-Union Meeting on Charged-Particle Accelerators* [in Russian], Vol. 2 (Nauka, Moscow, 1975), p. 309; Part. Accel. **7**, 197 (1976); At. Energ. **40**, 49 (1976).
[6] V. I. Kudelaĭnen, I. N. Meshkov, and R. A. Salimov, Preprint 70-72,

Nuclear Physics Institute, Novosibirsk (1970) [in Russian]; Preprint 77-08, Part B, CERN, Geneva (1977).
[7] V. V. Anashin, G. I. Budker, N. S. Dikanskiĭ *et al.*, in *Proc. of the Fourth All-Union Meeting on Charged-Particle Accelerators* [in Russian], Vol. 2 (Nauka, Moscow, 1975), p. 308.
[8] G. I. Budker, A. F. Bulyshev, and N. S. Dikanskiĭ, in *Proc. of the Fifth All-Union Meeting on Charged-Particle Accelerators* [in Russian], Vol. 1 (Nauka, Moscow, 1977), p. 236; Preprint 76-92, Nuclear Physics Institute, Novosibirsk (1976) [in Russian].
[9] G. I. Budker and A. N. Skrinskiĭ, Usp. Fiz. Nauk **124**, 561 (1978) [Sov. Phys. Usp. **21**, 277 (1978)].
[10] G. I. Derbenev and A. N. Skrinskiĭ, Fiz. Plazmy **4**, 492 (1978) [Sov. J. Plasma Phys. **4**, 273 (1978)].
[11] M. Bell, J. Chaney, H. Herr *et al.*, Nucl. Instrum. Methods **190**, 237 (1981).
[12] T. Ellison, W. Kells, V. Kerner *et al.*, IEEE Trans. Nucl. Sci. **NS-30**, 2370 (1983).
[13] E. N. Demen't'ev, N. S. Dikanskiĭ, A. C. Medvedko *et al.*, Preprint 79-70, Nuclear Physics Institute, Novosibirsk (1979) [in Russian]; Preprint 79-41, CERN/PS/AA, Geneva (1979).
[14] V. V. Parkhomchuk and D. V. Pestrikov, Zh. Tekh. Fiz. **50**, 1411 (1980) [Sov. Phys. Tech. Phys. **25**, 875 (1980)].
[15] G. I. Budker, N. S. Dikanskiĭ, I. N. Meshkov *et al.*, in *Proc. of the Tenth Intern. Conf. on Accelerators of High-Energy Charged Particles* [in Russian], Vol. 2, p. 141 (1978).
[16] D. Moehl, G. Petrucci, L. Thorndahl *et al.*, Phys. Rep. **58**, 367 (1980).
[17] B. Franzke, in *Proc. of the Third European Particle Accelerator Conf.*, Berlin, 1992, Vol. I, p. 367.
[18] A. S. Artamonov, Ya. S. Derbenev, and E. L. Saldin, Part. Accel. **23**, 79 (1988).
[19] Ya. S. Derbenev and A. N. Skrinskiĭ, Preprint 79-87, Nuclear Physics Institute, Novosibirsk (1979) [in Russian].
[20] Ya. S. Derbenev and A. N. Skrinsky, Sov. Phys. Rev. **3**, 165 (1981).
[21] B. I. Trubnikov, in *Problems of Plasma Theory* [in Russian], Part 1 (Gosatomizdat, Moscow, 1963), p. 157.
[22] L. D. Landau, Zh. Eksp. Teor. Fiz. **7**, 203 (1937) [in Russian].
[23] N. S. Dikanskiĭ, V. I. Kudelaĭnen, V. A. Lebedev *et al.*, Preprint 88-61, Nuclear Physics Institute, Novosibirsk (1988) [in Russian].
[24] V. V. Parkhomchuk, in *Proc. of the Workshop on Electron Cooling and Related Applications*, Kernforschungszentrum Karlsruhe, 1984, p. 71.
[25] I. N. Meshkov, in *Proc. of the Workshop on Beam Cooling and Related Topics*, Montreaux, 1993, CERN, Geneva, 1994, p. 26.
[26] Ya. S. Derbenev and I. N. Meshkov, Preprint 77-08, CERN, Geneva (1977).
[27] H. Poth, Preprint EP/77-08, CERN, Geneva (1990).
[28] N. S. Dikanskiĭ, V. I. Kononov, V. I. Kudelaĭnen *et al.*, in *Proc. of the Sixth All-Union Meeting on Charged-Particle Accelerators* [in Russian], Vol. 1, JINR, Dubna, 1979, p. 99.
[29] H. F. Beyer, D. Ziesen, O. Guzman *et al.*, Part. Accel. **24**, 163 (1989).
[30] N. S. Dikanskiĭ, V. I. Kokoulin, N. Kh. Kot *et al.*, in *Proc. of the Thirteenth All-Union Conference on High-Energy Particle Accelerators* [in Russian], Vol. 1 (Nauka, Novosibirsk, 1987), p. 330.
[31] V. V. Parkhomchuk and A. N. Skrinsky, Rep. Prog. Phys. **54**, 919 (1991).
[32] J. Bosser, CERN Accelerator School, CERN 92-01, Geneva (1992).
[33] A. Wolf, C. Ellert, M. Grieser *et al.*, in *Proc. of the Workshop on Beam Cooling and Related Topics*, Montreaux, 1993, CERN, Geneva, 1994, p. 416; A. Wolf, *Wechselwirkung zwischen hochgeladen Ionen und freien Electronen*, Univ. Heidelberg, 1992.
[34] M. Grieser, F. Albrecht, D. Habs *et al.*, in *Report on the Fourth European Particle Accelerator Conf.*, London, 1994.
[35] H. Danared, in *Proc. of the Workshop on Beam Cooling and Related Topics*, Montreaux, 1993, CERN, Geneva, 1994, p. 322.
[36] C. Ellert, D. Habs, E. Jaeschke *et al.*, Nucl. Instrum. Methods A **314**, 399 (1992).
[37] T. Ellison, M. Ball, B. Brown *et al.*, *Scientific and Technical Report of Indiana Univ. Cyclotron Facility*, Indiana Univ., Bloomington, 1990, p. 112.
[38] M. Steck, K. Beckert, F. Bosch *et al.*, in *Report on the Fourth European Particle Accelerator Conf.*, London, 1994.
[39] L. D. Landau and E. M. Lifshitz, *Statistical Physics*, 2nd ed. (Pergamon Press, Oxford, 1969) [Russian original of later edition, Nauka, Moscow, 1976].
[40] I. N. Meshkov, *Transport of Charged-Particle Beams* [in Russian] (Nauka, Novosibirsk, 1991).
[41] V. I. Kudelaĭnen, V. A. Lebedev, I. N. Meshkov *et al.*, Zh. Eksp. Teor. Fiz. **83**, 2056 (1982) [Sov. Phys. JETP **56**, 1191 (1982)].
[42] I. Hofmann, in *Proc. of the Workshop on Beam Cooling and Related Topics*, Montreaux, 1993, CERN, Geneva, 1994, p. 330.
[43] H. Bruck, *Accélérateurs Circulaires de Particules* (Presses Universitaires de France, Paris, 1966) [Russian transl., Atomizdat, Moscow, 1970].
[44] M. Steck, N. Angert, K. Beckert *et al.*, in *Proc. of the Third European Particle Accelerator Conf.*, Berlin, 1992, Vol. I, p. 827; in *Proc. of the Workshop on Beam Cooling and Related Topics*, Montreaux, 1993, CERN, Geneva, 1994, p. 395.
[45] B. Hochadel, F. Albrecht, M. Grieser *et al.*, in *Proc. of the Workshop on Beam Cooling and Related Topics*, Montreaux, 1993, CERN, Geneva, 1994, p. 198.
[46] A. Piwinski, in *Proc. of the Ninth Intern. Conf. on High Energy Accelerators*, Stanford, 1974, p. 405.
[47] G. Kalish, K. Beckert, B. Franzke *et al.*, in *Proc. of the Third European Particle Accelerator Conf.*, Berlin, 1992, Vol. I, p. 780.
[48] T. Tanabe, I. Katayama, N. Inoue *et al.*, in *Proc. of the Workshop on Beam Cooling and Related Topics*, Montreaux, 1993, CERN, Geneva, 1994, p. 312.
[49] J. Bosser, M. Chanel, R. Ley, and G. Tranquille, in *Proc. of the Workshop on Physical Experiments and First Results on the Heavy Ion Storage and Cooler Rings*, Smolenice, 1992 (JINR, Dubna, 1994).
[50] V. V. Parkhomchuk and D. V. Pestrikov, in *Proc. of the Workshop on Physical Experiments and First Results on the Heavy Ion Storage and Cooler Rings*, Smolenice, 1992 (JINR, Dubna, 1994).
[51] A. G. Ruggiero, in *Proc. of the Workshop on Beam Cooling and Related Topics*, Montreaux, 1993, CERN, Geneva, 1994, p. 274.
[52] J. P. Schiffer, in *Proc. of the Workshop on Beam Cooling and Related Topics*, Montreaux, 1993, CERN, Geneva, 1994, p. 455.
[53] Yu. Ts. Oganessian, O. N. Malyshev, I. N. Meshkov *et al.*, Z. Phys. A **341**, 217 (1992).
[54] The collection *The Heavy-Ion Storage Complex K4–K10* [in Russian], JINR, Dubna (1992).
[55] P. Lefevre and D. Moehl, in *Proc. of the Workshop on Beam Cooling and Related Topics*, Montreaux, 1993, CERN, Geneva, 1994, p. 411.
[56] R. N. Sagaĭdak, in *Proc. of the Third European Particle Accelerator Conf.*, Berlin, 1992, Vol. I, p. 32.
[57] E. Asseo, S. Baird, J. Bosser *et al.*, in *Proc. of the Third European Particle Accelerator Conf.*, Berlin, 1992, Vol. I, p. 449.
[58] T. Bergmark, C. Ekstroem, C.-J. Friden *et al.*, in *Proc. of the Third European Particle Accelerator Conf.*, Berlin, 1992, Vol. I, p. 465.
[59] Yu. Ts. Oganesyan and G. M. Ter-Akop'yan, in *Proc. of the Third European Particle Accelerator Conf.*, Berlin, 1992, Vol. I, p. 13.
[60] Yu. É. Penionzhkevich, Fiz. Elem. Chastits At. Yadra **25**, 930 (1994) [Phys. Part. Nucl. **25**, 394 (1994)].
[61] Y. Fujita, J. Trotscher, H. Wollnik *et al.*, in *Proc. of the Symp. on Structure and Reactions of Unstable Nuclei*, Nigata, Japan, 1991, p. 40.
[62] I. N. Meshkov and A. N. Skrinskiĭ, see I. N. Meshkov, Doctoral Dissertation, Nuclear Physics Institute, Siberian Division, USSR Academy of Sciences, Novosibirsk, 1975 [in Russian].
[63] G. M. Ter-Akop'yan, private communication, JINR, Dubna (1994).
[64] H. Eickhoff, K. Beckert, F. Bosch *et al.*, in *Proc. of the Workshop on Beam Cooling and Related Topics*, Montreaux, 1993, CERN, Geneva, 1994, p. 310.
[65] R. Grimm, N. Grieser, A. Gruber *et al.*, in *Proc. of the Workshop on Beam Cooling and Related Topics*, Montreaux, 1993, CERN, Geneva, 1994, p. 39.
[66] D. Moehl, *Report on the Discussion Meeting on Cold Stored Ion Beams*, Max-Planck-Institut für Kernphysik, Heidelberg, July 1994.
[67] N. V. Karlov, *Lectures on Quantum Electronics* [in Russian] (Nauka, Moscow, 1983), p. 21.
[68] V. B. Berestetskiĭ, E. M. Lifshitz, and L. P. Pitaevskiĭ, *Relativistic Quantum Theory* (Pergamon Press, Oxford, 1971) [Russian original, Part 1, Nauka, Moscow, 1968, p. 278].
[69] *Working Meeting on the Use of Lasers for Studying Atomic Nuclei* [in Russian], Dubna, 1990 (JINR, Dubna, 1991); A. Ya. Anastasov, Yu. P. Gangrskiĭ, B. N. Markov *et al.*, Zh. Eksp. Teor. Fiz. **105**, 250 (1994) [JETP **78**, 132 (1994)].
[70] R. Giannini, P. Lefevre, and D. Moehl, Preprints CERN/PS 87-103, 87-107, Geneva (1987).
[71] T. Ellison, Part. Accel. (1994) [in press].
[72] G. I. Budker, T. A. Vsevolozhskaya, N. S. Dikanskiĭ *et al.*, in *Proc. of the*

Fifth All-Union Meeting on Charged-Particle Accelerators [in Russian], Vol. 1 (Nauka, Moscow, 1977), p. 299.
[73] H. Poth, Appl. Phys. A **43**, 287 (1987).
[74] I. N. Meshkov, Report presented at the seminar of the PS/AR Division, CERN, 1993.
[75] Yu. L. Sokolov *et al.*, Nuovo Cimento **14D**, 183 (1992).
[76] V. V. Parkhomchuk, in *Proc. of the Symposium Antimatter-87*, Karlsruhe, 1987.
[77] M. Charlton, J. Eades, and D. Horvath *et al.*, Physics Reports, V. 241, No. 2, p. 67 (1994).

Translated by Patricia A. Millard